TO APPEAR IN APJ: 20 MARCH 2001
Preprint typeset using LaTeX style emulateapj v. 26/01/00

STELLAR MASS-TO-LIGHT RATIOS AND THE TULLY-FISHER RELATION

ERIC F. BELL AND ROELOF S. DE JONG[1]
Steward Observatory, University of Arizona, 933 N. Cherry Ave., Tucson, AZ 85721, USA

TO APPEAR IN APJ: *20 March 2001*

ABSTRACT

We have used a suite of simplified spectrophotometric spiral galaxy evolution models to argue that there are substantial variations in stellar mass-to-light ratios (M/Ls) within and among galaxies, amounting to factors of between 3 and 7 in the optical, and factors of 2 in the near-infrared. Our models show a strong correlation between stellar M/L and the optical colors of the integrated stellar populations. Under the assumption of a universal spiral galaxy IMF, relative trends in model stellar M/L with color are robust to uncertainties in stellar population and galaxy evolution modeling, including the effects of modest bursts of star formation. Errors in the dust reddening estimates do not strongly affect the final derived stellar masses of a stellar population. We examine the observed maximum disk stellar M/Ls of a sample of spiral galaxies with accurate rotation curves and optical and near-infrared luminosity profiles. From these observed maximum disk M/Ls we conclude that a Salpeter Initial Mass Function (IMF) has too many low-mass stars per unit luminosity, but that an IMF similar to the Salpeter IMF at the high-mass end with less low-mass stars (giving stellar M/Ls 30% lower than the Salpeter value) is consistent with the maximum disk constraints. Trends in observed maximum disk stellar M/Ls with color provide a good match to the predicted model relation, suggesting that the spiral galaxy stellar IMF is universal and that a fraction of (particularly high surface brightness) spiral galaxies may be close to maximum disk. We apply the model trends in stellar M/L with color to the Tully-Fisher (TF) relation. We find that the stellar mass TF relation is relatively steep and has modest scatter, and is independent of the passband and color used to derive the stellar masses, again lending support for a universal IMF. The difference in slope between the optical (especially blue) and near-infrared TF relations is due to the combined effects of dust attenuation and stellar M/L variations with galaxy mass. Assuming the HST Key Project distance to the Ursa Major Cluster and neglecting the (uncertain) molecular gas fraction, we find that the baryonic TF relation takes the form $M_{\rm baryon} \propto V^{3.5}$ (with random and systematic 1σ slope errors of ~ 0.2 each) when using a bisector fit and rotation velocities derived from the flat part of the rotation curve. Since we have normalized the stellar M/Ls to be as high as can possibly be allowed by maximum disk constraints, the slope of the baryonic TF relation will be somewhat shallower than 3.5 if all disks are substantially sub-maximal.

Subject headings: galaxies : spiral — galaxies : stellar content — galaxies : evolution — galaxies : fundamental parameters

1. INTRODUCTION

The stellar mass-to-light ratio (M/L) is an important parameter in astrophysics as it allows translation between photometry and dynamics. The stellar M/L has a direct bearing on two hotly debated areas in spiral galaxy research: the appropriate stellar M/Ls to be used for spiral galaxy rotation curve decompositions, and the passband-dependent slope of the galaxy magnitude-rotation velocity relation (Tully & Fisher 1977, TF relation hereafter). In this paper, we address the stellar M/Ls of spiral galaxies, briefly explore the implications of our results for rotation curve decompositions and investigate in more depth the slope of the TF relation.

There is presently much interest in decomposing spiral galaxy rotation curves into contributions from the gaseous, stellar and dark matter contents (e.g. Verheijen 1997; de Blok & McGaugh 1998). The primary motivation for this interest is that, in principle, the structure of dark matter halos can be determined from spiral galaxy rotation curves *if* the contribution from gas and stars can be properly understood. In turn, the structure of dark matter halos is a strong constraint on dark matter halo formation models (e.g. Moore et al. 1998; Navarro & Steinmetz 2000a). The main challenge in determining the dark matter contribution to a given rotation curve is our ignorance regarding plausible values of the stellar M/L: the gas contribution is typically well-understood and relatively small (Verheijen 1997; Swaters, Madore & Trewhella 2000). The situation is degenerate enough that many rotation curves can be equally well-fit by models in which the central parts of the rotation curve are dominated entirely by stellar mass or by dark matter (e.g. van Albada et al. 1985; Swaters 1999). In order to resolve this degeneracy, some independent constraints on stellar M/Ls, and their variations with radius and galaxy properties, are required.

The implications of the stellar M/L for the TF relation are no less important. The TF relation relates the integrated luminosity in a given passband to the global dynamics of the galaxy and its dark matter halo. The dust-corrected TF relation has a slope which steepens towards redder passbands (going between $L \propto V^3$ or shallower in the optical to $L \propto V^4$ in the near-infrared; Verheijen 1997; Tully et al. 1998) indicating that there is a trend in color and stellar M/L with galaxy mass. This change in slope with passband can considerably weaken the power of the TF relation as a test of galaxy formation and evolution models (such as those by Cole et al. 2000; Navarro & Steinmetz 2000b; van den Bosch 2000): it is possible to reproduce the TF relation in one passband easily without reproducing the TF relation in other passbands (for a multi-waveband comparison of models with the TF relation see e.g. Heavens & Jimenez 1999).

One way around this confusion is to explore the total baryonic mass TF relation. An estimate of the baryonic TF relation can be obtained by adding the gas mass to a crude estimate of stellar mass implied by the luminosity (usually assuming a

constant M/L). This has been attempted the most thoroughly by McGaugh et al. (2000) using a constant M/L in *B*, *I*, *H*, and *K* bands, although e.g. Milgrom & Braun (1988) and Matthews, van Driel & Gallagher (1998) discussed aspects of this problem. Because the stellar M/L is likely to vary along the TF relation in all passbands, their composite baryonic TF relation will have a larger scatter and different slope than the true baryonic TF relation. A deeper and firmer understanding of the baryonic TF relation is only possible once variations in stellar M/L along the TF relation are understood and incorporated in the analysis.

In this paper, we use simplified spiral galaxy evolution models similar to the ones presented by Bell & Bower (2000) to investigate plausible trends in stellar M/L with galaxy properties, assuming a universal IMF. We discuss these models briefly in §2. In §3 we investigate trends in spiral galaxy stellar M/L for a number of plausible models, finding that there are systematic variations in stellar M/L as a function of many galaxy parameters, and that stellar M/Ls correlate most tightly with galaxy color. In §4 we investigate the physical basis of the color–M/L relation and we discuss uncertainties in the stellar M/Ls, including the effects of using different stellar population models, different IMFs, different galaxy evolution prescriptions, and dust. In §5 we discuss the implications of these variations in stellar M/L for rotation curve decompositions, and put the stellar M/Ls onto an observationally-determined maximum-disk scale. In §6 we then discuss at length the implications of these variations in stellar M/L for the stellar mass and baryonic TF relation. Finally, in §7, we present our conclusions. Readers not interested in the details of the models and a detailed analysis of the uncertainties in model stellar M/Ls can skip §§2 and 4. Note that we state all stellar M/Ls in solar units. We adopt the HST Key Project distance scale in this paper, corresponding to $H_0 = 71$ km s^{-1} Mpc^{-1} (Sakai et al. 2000).

2. THE GALAXY EVOLUTION MODELS

To construct the model M/Ls for spiral galaxies, we use models similar to those presented by Bell & Bower (2000). They presented a suite of simple spectrophotometric disk evolution models designed to reproduce many of the trends between the radially-resolved colors of spiral galaxies and their structural parameters, as observed by Bell & de Jong (2000). These models were not designed to address the evolution of bulges or dwarf Spheroidal galaxies: the star formation laws used in these models (parameterized using surface density) are valid only for disk-dominated galaxies. These models describe the evolution of a gaseous disk, according to a prescribed star formation law and chemical evolution prescription (assuming the instantaneous recycling approximation; IRA). Relaxing the IRA would have two effects: it would allow non-solar abundance ratios to develop, and it would slightly modify the time evolution of the metallicity of galaxies. Most stellar population models are incapable of dealing adequately with non-solar abundance ratios: however, it looks likely that the effects of non-solar abundance ratios on integrated colors are modest (as they mimic the effects of modest changes in metallicity; e.g. Salasnich et al. 2000). Furthermore, the time evolution of spiral galaxy metallicity (which is dominated, by mass, by the Type II supernova product oxygen) is described fairly accurately by the IRA except at late stages of galactic evolution near gas exhaustion (e.g. Tinsley 1980; Pagel 1998; Portinari & Chiosi 1999; Prantzos & Boissier 2000). Thus, our use of the IRA is a reasonable approximation, bearing in mind the modest effects caused by adopting it, and the considerable stellar population and galaxy evolution modeling uncertainties.

To construct radially-resolved stellar population colors, the stellar populations synthesis (SPS) models of Bruzual & Charlot (2001), as described in Liu, Charlot & Graham (2000) are used, adopting a Salpeter (1955) IMF, which we modify by globally scaling down its stellar M/L by a factor of 0.7 (cf. Fukugita, Hogan, & Peebles 1998). We adopt lower and upper mass limits of $0.1M_\odot$ and $125M_\odot$ respectively. In Bell & Bower (2000) we adopted a pure Salpeter (1955) IMF: in this paper, we have been forced to adopt an IMF with lower M/Ls to agree with observational maximum disk M/L constraints (see §5). This global reduction in stellar M/L is essentially the same as adopting an IMF with with fewer low-mass stars, as the low mass stars contribute only to the mass, but not the luminosity or color, of the stellar population. It is interesting to note that there is increasing empirical evidence for a universal IMF with a Salpeter slope for stars more massive than the Sun, and a shallower slope for stars less massive than the Sun (Kroupa 2000). This IMF has stellar M/Ls comparable to or slightly lower than the maximum disk-scaled IMF we adopt in this paper. It is important to note that neither the slope nor the scatter of the stellar M/Ls, nor the trends in color with galaxy properties are affected by our adoption of a scaled-down Salpeter IMF: the only effect on the following analysis is to modify the overall normalization of the stellar M/Ls.

For our models, we follow the evolution of an exponential gaseous disk using either a Schmidt (1959) local gas density-dependent star formation law or a gas density- and dynamical time-dependent star formation law (Kennicutt 1998). Model galaxies with a wide range of masses and central surface densities are generated, as we do not attempt to *a priori* predict the mass and central surface density distributions of spiral galaxies. To avoid comparing the observed galaxies to model galaxies without any observed analogue from Bell & de Jong (2000), we select model galaxies to have a similar range in *K* band absolute magnitudes and central surface brightnesses as their observed galaxies (including an observed modest absolute magnitude–central surface brightness correlation). These models are tuned to reproduce observed trends in color-based local age and metallicity as a function of local *K* band surface brightness, in conjunction with the observed correlation between gas fraction and *K* band central surface brightness (Bell & de Jong 2000; Bell & Bower 2000).

We present a total of six models in this paper. i) We first use a closed box model, with no gas infall or outflow, a galaxy age of 12 Gyr and a Schmidt star formation law. The main disadvantages of this model is the lack of a strong metallicity-magnitude correlation and weaker age–magnitude correlation, and the underprediction of the age gradients. We then allow ii) gas infall (whose timescale depends on galaxy mass and radius) *or* iii) metal-enriched outflow, both of which alleviate the above shortcomings of the closed-box model. iv) We then adopt a dynamical time-dependent star formation law (without infall or outflow), which we find produces a 'backwards' metallicity–magnitude correlation, and is therefore unacceptable, in isolation. v) We then explore the use of a mass-dependent galaxy formation epoch without infall or outflow, which imprints metallicity–magnitude and age–magnitude correlations. A mass-dependent formation epoch is a common feature of many cosmologically-motivated galaxy formation models (e.g. Somerville & Primack 1999; Cole et al. 2000). vi) Finally, we explore a 'burst' model with a mass-dependent galaxy

formation epoch and no infall or outflow, where the star formation rate is varied on 0.5 Gyr timescales with a log-normal distribution with a factor-of-two width. None of these models perfectly describe the trends in spiral galaxy colors with galaxy parameters observed in Bell & de Jong (2000); however, the models taken as a suite encompass the range of behaviors seen in the observed galaxy sample. We adopt the mass-dependent formation epoch model with bursts, with a scaled-down Salpeter IMF, as the default model. This model reproduces the trends in local spiral galaxy age and metallicity with local K band surface brightness with acceptable scatter, while simultaneously reproducing the age–magnitude and metallicity–magnitude correlations with acceptable scatter. However, as we later demonstrate (see e.g. §4.3 and Fig. A10), the choice of model does not significantly affect any of our conclusions. For more model details, see Bell & Bower (2000).

3. CONSTRUCTING MODEL MASS-TO-LIGHT RATIOS

We use the spiral galaxy evolution models (which reproduce the trends in spiral galaxy color with structural parameters) to construct stellar M/Ls for integrated stellar populations. These are converted into solar units assuming solar absolute magnitudes of 5.47, 4.82, 4.46, 4.14, and 3.33 in Johnson B and V, Kron-Cousins R and I, and Johnson K passbands respectively (Cox 2000; Bessel 1979). We also adopt Johnson J and H band solar absolute magnitudes of 3.70 and 3.37 respectively from Worthey (1994) as Cox (2000) does not present J and H band magnitudes of the Sun: Worthey (1994) magnitudes in other passbands are comparable to those presented by Cox (2000). Instead of using the full gas mass loss histories from the SPS models, we used the IRA to construct the stellar masses. This may lead to errors of $\lesssim 5$ per cent in stellar M/L (compared to the exact value). Bearing in mind the size of variations in M/L the model predicts (greater than a factor of two), and the other considerable uncertainties affecting the stellar M/Ls, such as the stellar initial mass function (IMF) and dust, our use of the IRA is more than acceptable.

We show an example of the stellar M/Ls of our model galaxies for the mass-dependent formation epoch with bursts model in Fig. 1. We show this particular model for two reasons. Firstly, this model provides the best match to the overall observed galaxy properties. Secondly, and more importantly, this model shows the most scatter of any of our models, but has quantitatively the same overall behavior as all of our models (see e.g. §4.3 and Fig. A10). We show the trends in stellar M/L in the B band (open circles) and K band (filled circles) as a function of K band absolute magnitude (a), K band central surface brightness (b), gas fraction (c), and B–R galaxy color (d). Results for other models are presented in Appendix A.

One obvious conclusion is that there are significant trends in model stellar M/L with all four depicted galaxy parameters *in all passbands, even in the K band*. The trends amount to factors of ~ 7 in B, ~ 3 in I, and ~ 2 in K for plausible ranges of galaxy parameters. This firmly dispels the notion of a constant stellar M/L for a spiral galaxy in any passband: this conclusion is even true in K band, where there have been claims that the stellar M/L will be robust to differences in star formation history (SFH; e.g. de Jong 1996; Verheijen 1997). Of course, we find that the trends in stellar M/L are minimized in K band: this suggests that K band observations are important for any observations in which minimizing scatter in M/L is important (e.g. for rotation curve studies).

The scatter in model stellar M/L at a given magnitude is

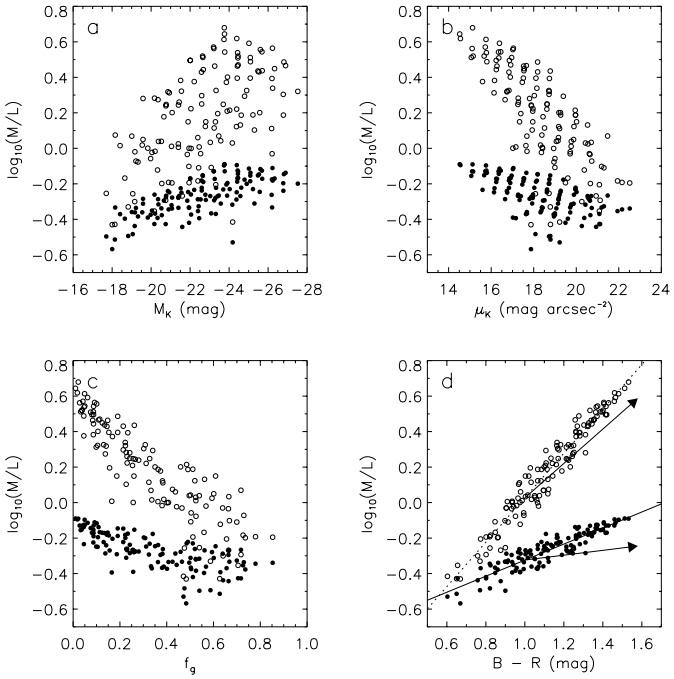

FIG. 1.— Trends in model stellar M/Ls with galaxy parameters for the formation epoch model with bursts. We show the trends in model stellar M/L in the B band (open circles) and K band (filled circles) as a function of K band absolute magnitude (a), K band central surface brightness (b), gas fraction (c), and $B-R$ galaxy color (d). In panel d, we also show the fit to the variation of model stellar M/L with B–R color for this model in B (dotted line) and K (solid line) and dust extinction vectors in B and K band (arrows) following Tully et al. (1998). The dust extinction vectors represent the correction to face-on suffered by a Milky Way-type galaxy viewed at an inclination of 80 degrees.

rather large as a consequence of the modeling assumptions. The SFH of our model galaxies depends primarily on their local surface density, and only weakly on their total mass, as is observed (Bell & de Jong 2000). As galaxies come in a range of surface brightnesses at a given magnitude (de Jong & Lacey 2000), our models will have a range of SFHs and consequently M/Ls at a given magnitude. There is considerable scatter in stellar M/L with K band central surface brightness and with gas fraction; however, this scatter is highly model dependent as there is no scatter in these relations for the closed box models, and intermediate scatter for the outflow and infall models.

One important conclusion is that, for all the models investigated for this paper, the model stellar M/Ls in all optical and near-infrared (near-IR) passbands correlate strongly, with minimal scatter, with galaxy color (see also Bottema 1997). This is expected: the star formation and chemical enrichment history determine both the stellar M/L and galaxy color. Later, we demonstrate that the slope of the stellar M/L–color correlation is very robust, and we place a strong constraint on the zero point of the correlation. This correlation is a powerful tool for understanding stellar M/Ls of spiral galaxies for use in e.g. rotation curve decompositions or in constructing passband-independent TF relations. We tabulate least-squares fits to the maximum disk-scaled color–stellar M/L relations in Table A3 of Appendix A for all models introduced in §2 and for a broad range in color combinations.

Using our models we predict, *under the assumption of a universal IMF*, that workers determining the stellar M/Ls of spiral galaxies (e.g. Bottema 1993, 1999; Swaters 1999; Weiner et al. 2000) will, with sufficient sample size and control of the

systematic uncertainties, observe trends in stellar M/L which correlate most tightly with galaxy color. In §5, we demonstrate that there are already indications from rotation curve studies that the correlation between M/L and color has been observed (see also Ratnam & Salucci 2000).

Another interesting implication of the tight correlation between stellar M/L and color is that, because color gradients are common in spiral galaxies, significant gradients in stellar M/L should be present in most spirals, in the sense that the outer regions of galaxies will tend to have lower stellar M/L than the inner regions of galaxies (assuming a universal IMF). Obviously this stellar M/L gradient will vary on a case-by-case basis. For many galaxies the assumption of a constant stellar M/L over the disk will not significantly affect mass decompositions using rotation curves, as in the outer regions (where the stellar M/L is lower) the stars contribute much less to the total mass than the dark matter (e.g. Weiner et al. 2000). Nevertheless, for accurate rotation curve studies, or studies based on e.g. B band photometry where the stellar M/L varies strongly as a function of color, the radial variation of stellar M/L should not be ignored lightly. A detailed study of spiral galaxy rotation curves, using these model stellar M/Ls, will be presented in our next paper.

4. HOW ROBUST ARE THE STELLAR MASS-TO-LIGHT RATIOS?

In the previous section, we made some strong claims about the stellar M/Ls of spiral galaxies. However, there are a number of uncertainties which may affect the model stellar M/Ls, such as uncertainties in SPS and galaxy evolution models, dust, and most importantly, the stellar IMF (and possible trends in IMF with galaxy type and structure). In the next sections, we discuss some of these uncertainties and the bearing of these on our results.

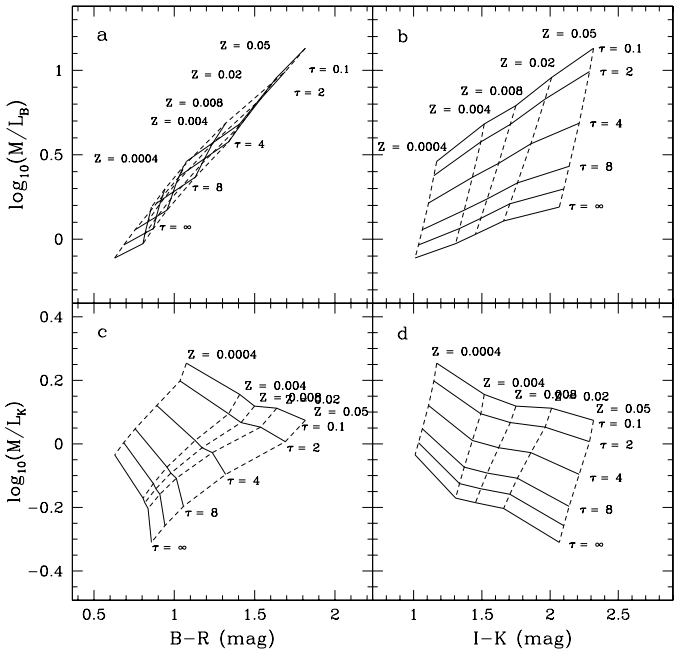

FIG. 2.— Trends in simple exponential SFH model stellar M/Ls with color. Stellar M/Ls for a Salpeter IMF in B (panels a and b) and K (panels c and d) of single metallicity exponentially declining star formation rate models from Bruzual & Charlot (2001) are shown against the model $B-R$ (panels a and c) and $I-K$ (panels b and d) broadband colors. Models of the same e-folding time scale τ have been connected by solid lines, models of the same metallicity Z are connected by dashed lines.

4.1. *The origin of the color–M/L correlation*

Before we can assess the uncertainties in the model color–M/L relations, we have to understand why the correlation between color and stellar M/L exists in the first place. To this end, we show in Fig. 2 color versus stellar M/L for a grid of exponentially declining star formation rate models. To construct model colors, we use SPS models with different metallicities from Bruzual & Charlot (2001). We use exponentially declining star formation rates as models with this type of SFH can reproduce the optical–near-IR colors of spiral galaxies quite naturally (e.g. Bell & de Jong 2000). Furthermore, a slowly declining or constant SFH is inferred for the solar neighborhood (e.g. Rocha-Pinto et al. 2000). The exponential decline in star formation rate is parametrized by e-folding timescale τ and the colors and M/Ls are evaluated after a lifetime of 12 Gyr. Models with different τ but the same metallicity are connected by solid lines, the same τs but different metallicities are connected by dashed lines.

When we consider the model grid for M/L in the B band versus $B-R$ color (Fig. 2, panel a), we can immediately see why the B band stellar M/L-color relation works so well. There is a tight correlation between $B-R$ color and stellar M/L independent of metallicity or SFH. Similar results are obtained for M/Ls in other optical passbands in combination with optical-optical colors.

The situation is slightly more complex when looking at trends in the K band stellar M/L with optical color (Fig. 2, panel c). The age (as parameterized by τ) and metallicity effects are no longer degenerate. However, realizing that chemical evolution caused by modest amounts of star formation raise the galaxy metallicity rapidly to at least 1/10th solar ($Z = 0.002$; in a closed box, conversion of $\sim$20% of the gas mass into stars raises the average stellar metallicity to over 0.1 solar), the range of relevant metallicities becomes narrower, and the color–M/L correlation becomes tighter. Still, we expect a bit more scatter in the relations in the K band, in particular for very young galaxies with nearly primordial metallicities (like SBS 1415+437: with a metallicity of 0.05 solar it is one of the lowest metallicity galaxies known; Thuan, Izotov & Foltz 1999).

We see that the method definitely breaks down when using $I-K$ versus M/L (Fig. 2, panels b and d). This is because we are now using a color that is mainly a metallicity tracer versus M/L, which is more sensitive to age effects. We therefore expect the method to work best with optical-optical color combinations (which are unfortunately most affected by dust). Even though the K band M/L –color relations are less tight, because of its much smaller dynamic range it is still the passband prefered for mass estimates, with I band providing an useful alternative.

4.2. *Stellar population model uncertainties and IMFs*

In the above analysis we used the SPS models of Bruzual & Charlot (2001) with a scaled-down Salpeter IMF, in conjunction with our own simple galaxy evolution models, to probe trends in stellar M/L with galaxy properties. However, the SPS models carry with them their own sets of uncertainties, such as the prescriptions for post-main sequence evolution and the relationship between stellar properties and the observable colors. For this reason, we compare the stellar M/Ls from a wide range of models here, to assess the robustness of our conclusions.

To test the consistency of the different SPS models (and later, the effect of different IMFs), we constructed a sequence of single-metallicity exponential SFH models with a range of

metallicities and exponential *e*-folding timescales. Then, for each SPS model, we compare the correlation between $B-R$ color and stellar M/L in a variety of passbands.

We show the effect of different SPS models in Fig. 3 and in Table A4 in Appendix A. We adopt a Salpeter IMF, and show the color–M/L relation for solar metallicity τ models in the B band (thin lines) and K band (thick lines). We show four SPS models: Bruzual & Charlot (2001, solid) models, Kodama & Arimoto (1997, dotted) models, Schulz et al. (2001, dashed) models and the updated PÉGASE models of Fioc & Rocca-Volmerange (2001, long dashed).

For all models we find very similar slopes and zero points for the color–M/L relation (to within 0.1 dex in M/L ; Fig. 3). This also holds true for other passband combinations and metallicities. The only exception to this result is the Schulz et al. (2001) model, which have an unusually bright asymptotic giant branch which produces very red optical–near-IR colors for solar metallicity stellar populations. The solar metallicity Schulz et al. (2001) model gives normal B band stellar M/Ls but very low K band stellar M/Ls, compared to the other solar metallicity models. Essentially, this means that the Schulz et al. (2001) solar metallicity model $B-K$ colors are redder than the other SPS models we compare to (and, indeed, most of the luminous spiral galaxies in our observational sample). This poses a problem, however, as at a given optical-optical color (e.g. $B-R$) the optical–near-IR colors (e.g. $B-K$) of the solar metallicity Schulz et al. (2001) models are far too red to explain observed galaxy colors, whereas the other models do reproduce the observed colors. In order to match observed spiral galaxy optical–optical and optical–near-IR colors simultaneously, 1/3 solar metallicity Schulz et al. (2001) models must be adopted. We plot these models in Fig. 3: these models have stellar M/Ls much closer to other models' solar metallicity stellar M/Ls. This slight model mismatch is actually quite useful: it demonstrates that even with substantial model differences, the stellar M/L at a given optical–near-IR color is robust to model differences.

We now test the effect of different IMFs in Fig. 4. We try out a wide range of IMFs for both the Bruzual & Charlot (2001) and PÉGASE models: Bruzual & Charlot (2001) models with a Salpeter IMF (with a logarithmic slope $x = -1.35$; solid), a Salpeter IMF modified to have a flat $x = 0$ slope below $0.6 M_\odot$ (dotted), and Scalo (1986) IMF (dashed); and the updated PÉGASE models of Fioc & Rocca-Volmerange (2001) with a steeper $x = -1.85$ IMF (long dashed) and a flatter $x = -0.85$ IMF (dot-dashed). All models have solar metallicity. The slopes of the color–M/L correlations are independent of IMF: only the zero-point is affected by the choice of IMF. The color range is also slightly affected by the IMF choice (especially the upper end of the IMF), as the range in models is from a single burst at the red end to constant star formation rate for 12 Gyr at the blue end. The sensitivity of the zero point of the color–M/L correlation to the IMF is due entirely to differences in the numbers of low mass stars in each IMF. These low mass stars significantly change the total mass of the stellar population, but hardly change the overall color and luminosity of the system (which is dominated by the more massive stars). This justifies the scaling of the Salpeter IMF that we have done to bring the stellar M/Ls of the Salpeter IMF into line with the maximum disk constraints in §5: this scaling has the same effect as a flattening of the low mass end of the IMF.

We therefore conclude that our choice of stellar population synthesis model does not significantly affect our conclusions: in particular, the *relative* trend in stellar M/L with color is preserved in all of the models which we examined. However, the model IMF does make a significant difference: while the IMF leaves the slope of the color–M/L correlation and the colors relatively unaffected, the IMF strongly affects the overall normalization of the stellar M/L.

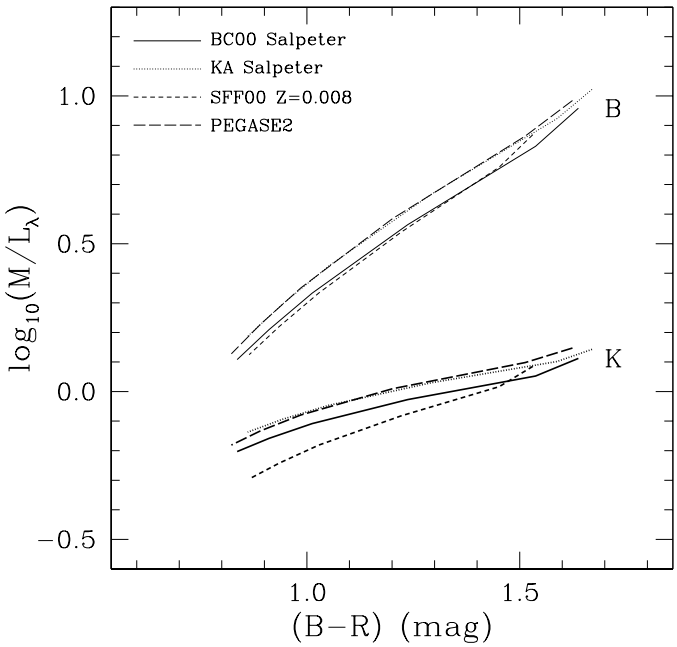

FIG. 3.— Comparison of the color–M/L relation for a sequence of exponentially declining star formation rate models of age 12 Gyr using a variety of SPS models. The red end of the lines represent a short burst of star formation, the blue end represents a constant star formation rate model. The thin lines are for M/L_B, the thicker lines are for M/L_K. The different models used are: Bruzual & Charlot (2001, solid), Kodama & Arimoto (1997, dotted), Schulz et al. (2001, dashed) and updated PÉGASE models of Fioc & Rocca-Volmerange (2001, long dashed) all with a Salpeter IMF. All models have solar metallicity except for the Schulz et al. (2001) models which have 1/3 solar metallicity (see text for more details).

4.3. *Galaxy evolution uncertainties*

In this section, we examine the uncertainties stemming from differences in galaxy evolution prescriptions. We have already examined the properties of six different galaxy evolution models in §3 and Appendix A. We found that there was little difference between the behaviors of the closed box, infall, outflow, dynamical time, mass-dependent formation epoch and mass-dependent formation epoch with bursts models. In particular, the trends in stellar M/L with color, and their zero-points, were remarkably robust to a variety of different effects, including low-level bursts in the SFH. In addition, we have tested the effects of changing the age of galaxies at the present day from 12 Gyr: age changes of ± 3 Gyr produce changes in model stellar M/L at a given color of only ± 0.05 dex.

One important issue is the effects of larger bursts: do galaxies with a recent or ongoing burst of star formation have stellar M/Ls which vary considerably from the stellar M/Ls of galaxies with more quiescent star formation but the same colors? We tested this case by adding a star burst with 0.5 Gyr duration to a range of exponential SFH models with a mass fraction of 10% of the total stellar mass formed over the lifetime of the galaxy. We viewed these models at a range of times after the burst, between 1 and 6 Gyr. A number of points are apparent from

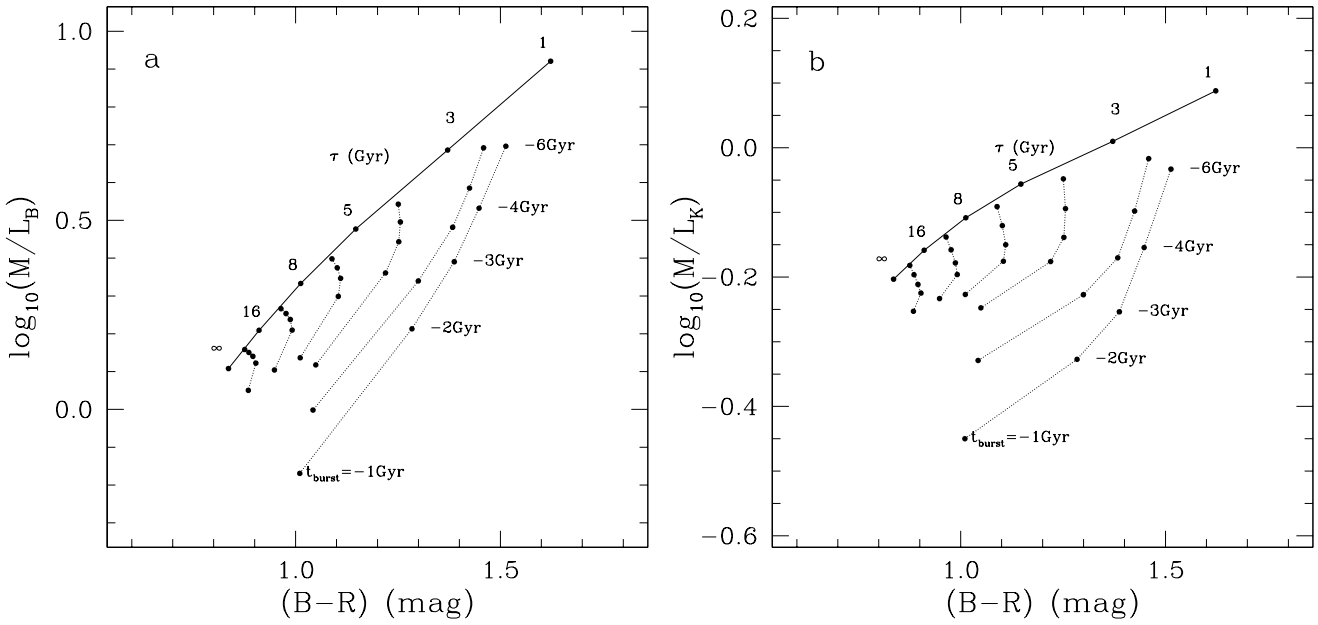

FIG. 5.— Color–M/L relations in B (a) and K (b) for a sequence of exponential declining star formation rate solar metallicity models of age 12 Gyr with 10% mass fraction added in 0.5 Gyr star bursts. The solid line connects the exponential SFH models with different e-folding times scales τ. The dotted lines connect models of the same τ value, but with added star bursts occuring 1, 2, 3, 4 or 6 Gyr ago.

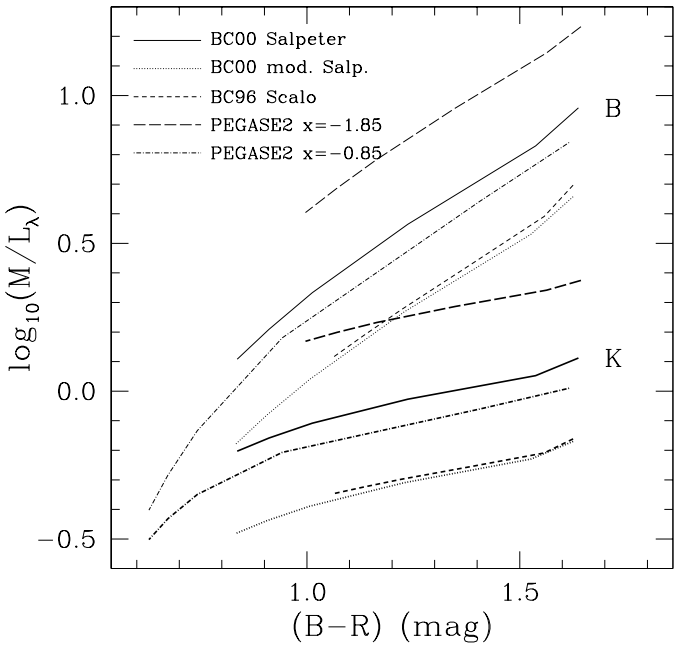

FIG. 4.— Comparison of the color–M/L relation for a sequence of exponentially declining star formation rate models of age 12 Gyr using a variety of IMFs. Again, the thin lines are for M/L_B, the thicker lines are for M/L_K. The different models and IMFs used are: Bruzual & Charlot (2001) models with a Salpeter x = –1.35 IMF (solid), a Salpeter IMF with x = 0 below 0.6$M_\odot$ (dotted), and Scalo (1986) IMF (dashed); and the updated PÉGASE models of Fioc & Rocca-Volmerange (2001) with a steeper x = –1.85 IMF (long dashed) and a flatter x = –0.85 IMF (dot-dashed). All models have solar metallicity.

inspection of Fig. 5. Firstly, the effects of a 10% burst of star formation are much larger for red earlier-type galaxies than for blue, later-type galaxies. This stems from the larger fractional contribution of the young stars to the total *luminosity* in redder galaxies. Secondly, maximum offsets from the color–stellar M/L correlation are expected to be ∼0.5 dex in B, and ∼0.3 dex in K band. Thirdly, bursts of star formation bias the stellar M/L to lower values at a given color. Finally, large effects are only visible for a period of ∼1 Gyr for bluer underlying stellar populations, but are visible for much longer (∼5 Gyr) for redder underlying stellar populations.

This at first sight seems discouraging: in particular, the sensitivity of the stellar M/L of redder underlying populations to a burst of star formation several Gyr ago implies significant scatter in the stellar M/Ls of redder galaxies. This is part of our motivation for choosing a model with bursts of star formation as our default: with a model which incorporates bursts of star formation, we can account for the lower stellar M/Ls of redder galaxies with even modest amounts of bursty star formation several Gyr ago (compare panels c and d of Fig. A10 in Appendix A). However, we can take some comfort from the fact that our use of a 10% burst is very conservative: recent bursts of star formation that large are unlikely, and are likely to be selected against in sample selection (by e.g. selecting for undisturbed and symmetric galaxies). Indeed, even if morphological selection does not filter out these galaxies, galaxies with such large bursts are expected to lie off of the TF relation (because their luminosities will have been considerably boosted by the starburst), and so may be selected against for this reason.

As a check, we have also examined the trends in stellar M/L with color using disk-dominated non-satellite galaxies from the heirarchical models of Cole et al. (2000). These models include the effects of halo formation and merging, gas cooling, star formation, feedback and dust (but use the same SPS models as we adopt for this paper, with a Kennicutt (1983) IMF and a 38% brown dwarf fraction), and therefore offer a completely independent assessment of the effects of galaxy evolution prescriptions on the stellar M/Ls of galaxies. The trend in their disk galaxy model stellar M/Ls with color is almost identical to those of the simpler models (in particular to the mass-dependent formation epoch with bursts model), albeit with more scatter due to the strongly irregular SFH (panel f of Fig. A10 of Appendix A). The key to the relatively modest scatter in model stellar M/L with color in their models can be linked to the

morphological transformations which accompany large mergers. Mergers large enough to produce large starbursts with large decreases in stellar M/L, are large enough to transform a disk-dominated into a spheroidal galaxy: these galaxies would not be included in any disk-dominated sample of galaxies.

We therefore conclude that choosing a different galaxy evolution prescription would not significantly affect the trends in model stellar M/L with color presented in this paper. Large bursts of recent star formation can lower the stellar M/L at a given color by up to a factor of three, however galaxies with a large amount of recent star formation are unlikely to feature heavily in a spiral galaxy sample. The lower-level bursts more typical of disk-dominated spiral galaxies add only modest amounts of scatter to the color–stellar M/L correlation and are accounted for by our default model.

4.4. *Dust*

Another potential concern is dust: dust simultaneously reddens and dims a stellar population, changing both axes in the correlation between color and stellar M/L. We address this problem in panel d of Fig. 1, where we show dust extinction vectors for the dust correction of Tully et al. (1998) in B and K band. Dust extinction vectors for screen and Triplex models (Disney, Davies & Phillipps 1989) are similar in direction to this vector. The dust vector shown in Fig. 1 represents a large effect: it is the correction to face-on suffered by a Milky Way-type galaxy viewed at an inclination angle of 80 degrees. For most galaxies the effects of extinction will be much smaller. It is clear that dust is a second order effect for estimating stellar M/Ls in this way. Dust extinguishes light from the stellar population, making it dimmer. However, dust also reddens the stellar population, making it appear to have a somewhat larger stellar M/L. To first order, these effects cancel out, leaving a dust-reddened galaxy on the same color–stellar M/L correlation. There is a possibility of overpredicting (underpredicting) the stellar M/L (thus the stellar mass) if not enough (too much) reddening correction is applied, as the reddening effect is larger than the extinction effect. However, even for the large extinction error illustrated here, the effect is of order 0.1–0.2 dex. This error is comparable to the errors from uncertainties in stellar population synthesis modelling and galaxy evolution prescriptions. However, this may not apply on a pixel-to-pixel level: some small regions of spiral galaxies may be optically thick in the optical, which completely obscures the light without producing any extra reddening (e.g. Witt, Thronson & Capuano 1992). Therefore, smaller scale applications of this color-based stellar M/L technique must be wary of the effects of dust.

4.5. *Summary*

The color–stellar M/L correlation is robust in a relative sense (both within a passband and between passbands), *provided there is no systematic change in IMF with galaxy type.* Model uncertainties, galaxy evolution prescription uncertainties, small bursts of star formation and dust uncertainties are all of order 0.1–0.2 dex or less. Large bursts of recent star formation may produce quite a large effect, depending on when they happen and on the properties of the underlying older stellar population. However, large bursts are unlikely to be common (at least at the present day: at higher redshift this need not be the case; e.g. Brinchmann & Ellis 2000). The IMF remains the largest uncertainty: assuming no trend in IMF with galaxy type, the range of IMFs presented in the literature causes uncertainty in the absolute normalization of the stellar M/Ls of at least a factor of two. We address this normalization in the next section.

5. ROTATION CURVES AND THE NORMALIZATION OF THE STELLAR M/L

We demonstrated that the model color–stellar M/L correlation is robust in a relative sense, but has uncertain overall normalization. For many applications, this is perfectly acceptable. For example, it is quite possible to investigate the *slope* of the stellar mass TF relation, or estimate the trend in stellar M/L as a function of galaxy radius for rotation curve fitting, without knowing the absolute normalization of the overall stellar M/L. However, for some applications, e.g. for understanding the slope of the *baryonic* TF relation, or in constraining the shape of dark matter haloes, it is important to understand both the relative trend of stellar M/L with color and the absolute normalization. The previous section showed that the question of the absolute normalization of the stellar M/L essentially boils down to one issue: the stellar IMF. To first order, the amount of stellar light produced by observationally plausible IMFs is rather similar; however, the slope of the IMF, especially at the low-mass end, changes the overall stellar mass considerably.

We cannot address this problem fully, short of counting all of the stars in spiral galaxies directly. However, we can provide some constraints. The rotation curves of spiral galaxies have contributions from the stellar mass, gas mass and dark matter. The relative contributions of each are difficult to estimate directly. However, interesting constraints can be derived by assuming that the mass of the stellar disk makes the maximum possible contribution to the rotation velocity: this is the maximum disk hypothesis (e.g. van Albada & Sancisi 1986). Fitting a maximal stellar disk to a rotation curve provides the maximum possible stellar M/L, thus providing a firm upper limit to the stellar M/Ls that we have constructed in the model.

We have examined the K band maximum disk stellar M/Ls of the Ursa Major Cluster sample of Verheijen (1997, Chapter 6), rescaled to the HST Key Project distance of 20.7 Mpc (Sakai et al. 2000) to place constraints on the normalization of the stellar M/Ls. This value is consistent (bearing in mind $\gtrsim$10% systematic uncertainties) with the distance derived from a different analysis of the Cepheid-calibrated TF relation (18.6 Mpc; Tully & Pierce 2000) and the brightness of a Type 1a supernova in NGC 3992 which was consistent with a distance of 24 ± 5 Mpc (Parodi et al. 2000). K band was adopted as we have shown above that using the K band results in the most robust stellar M/L estimation. We consider the maximum stellar M/L given by either the pseudo-isothermal or Hernquist halo fit. In Fig. 6 we plot this K band maximum disk stellar M/L against the $B-R$ color of the galaxy, de-reddened assuming dust extinction following Tully et al. (1998, see also §6). These are the dynamical upper limits for the stellar M/Ls of these galaxies, hence the upper limit signs.

NGC 4085 is highlighted: this nearly edge-on galaxy was observed with a beam the size of its minor axis diameter, resulting in the worst case scenario for beam smearing (e.g. van den Bosch et al. 2000). Consequently, it has a poorly resolved rotation curve, which biases the maximum disk M/L downwards. We ignore the stellar M/L estimate for NGC 4085 in the following discussion, although clearly a better resolved rotation curve would be useful.

The main point of this plot is that our SPS-based model stellar M/Ls should be the same as or lower than all of the observed

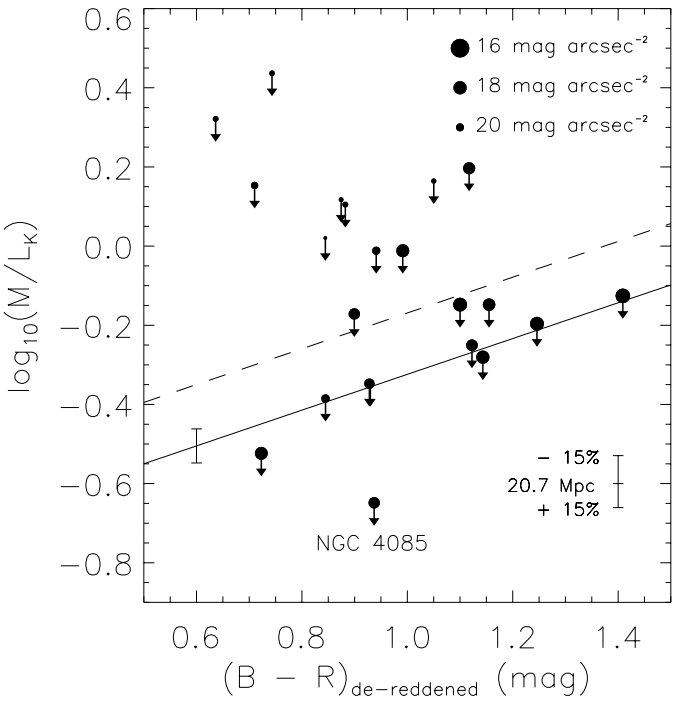

FIG. 6.— Observed K band maximum disk stellar M/Ls against de-reddened $B-R$ color. The data are from K band imaging and HI rotation curves from Verheijen (1997, Chapter 6), rescaled to a distance of 20.7 Mpc (Sakai et al. 2000): the effect on the maximum disk M/Ls of a $\pm$15% Ursa Major Cluster distance error is also shown. Overplotted is the least-squares fit to the correlation between color and stellar M/L for the formation epoch with bursts model assuming a Salpeter (dashed line) and a scaled-down Salpeter IMF (solid line). We also show the RMS spread of the formation epoch with bursts model around the color–M/L relation on the solid line as an error bar. NGC 4085 is highlighted: it has a poorly resolved rotation curve, which biases the maximum disk M/L downwards. Symbol size is coded by inclination-corrected K band central surface brightness.

maximum disk stellar M/Ls. We make the explicit assumption here that the lower envelope of the observed maximum disk stellar M/Ls is the meaningful constraint (again, we neglect NGC 4085 due to beam smearing). Galaxies with maximum disk M/Ls significantly above this envelope are interpreted as galaxies with significant dark matter within the optical radius of the galaxy: these galaxies are sub-maximal. This interpretation is supported by the surface brightnesses of the sub-maximal disks: they are all fairly low surface brightness. Low surface brightness galaxies are thought to have high maximum disk stellar M/Ls because they are dark matter dominated even in their inner regions (e.g. Verheijen 1997; de Blok & McGaugh 1998).

From Fig. 6, it is clear that applying our standard color–stellar M/L relation assuming a Salpeter x = 1.35 IMF normalization over-predicts the stellar M/L of many of the galaxies (dashed line). Motivated by recent IMF determinations which suggest a turn-over in the IMF at low stellar masses (e.g. Kroupa, Tout & Gilmore 1993; Larson 1999; Kroupa 2000) we scale down the Salpeter IMF masses by a factor of 0.7. This is equivalent to a Salpeter IMF x = 1.35 with a flat x = 0 slope below 0.35M$_\odot$, or a Kennicutt (1983) IMF with a brown dwarf fraction of $\sim$ 40%. This scaled IMF results in the solid line in Fig. 6. This IMF is maximal: the stellar M/Ls can be no larger than those predicted by a model adopting this IMF, modulo distance uncertainties. The maximum disk M/Ls scale inversely with distance: a 15% error bar for the data points is shown, corresponding to a 10% random and 10% systematic error added in quadrature (Sakai et al. 2000). Indeed, the stellar M/Ls might have to be even somewhat lower: all disks may be sub-maximal (e.g. Bottema 1997; Courteau & Rix 1999), the K band maximum disk stellar M/L has not been corrected for the effects of dust extinction, and the mass locked up in molecular hydrogen has not been accounted for in these rotation curve decompositions. On the other hand, the HI rotation curves are all to some extent affected by at least small amounts of beam smearing (which would work to lower the maximum disk stellar M/L estimate): the upshot is that there is some scope for moving the stellar M/Ls only slightly upwards, and there is much scope for moving the stellar M/Ls substantially downwards, lending credibility to the idea that our scaled Salpeter IMF is maximal.

One remarkable point is that, modulo the modest sample size, the slope of the lower envelope of the observational maximum disk stellar M/Ls is accurately described by the predicted trend in K band stellar M/L with $B-R$ color. The zero-point of the model has been constrained to match the data; however, there was no *a priori* reason that the slope of the observational color–stellar M/L relation needed to match the predictions of the model. This is remarkable for a few reasons. Firstly, it puts our proposition that the stellar M/L is primarily a function of color, varying a factor of two in the K band between the reddest and bluest galaxies, on a more empirical footing. Secondly, it suggests that galaxies close to maximum disk have very similar IMFs, as strong IMF variations with galaxy color should be easily visible in this plot. In fact, the scatter of the observational lower envelope around the predicted line is consistent with the predicted model scatter due to differences in SFH at a given color, leaving *no* freedom for random galaxy-to-galaxy IMF variations. Finally, it implies that the galaxies closest to the observed limit (high surface brightness galaxies in general), are probably close to maximum disk, because the adopted IMF already gives a reasonably low M/L zero-point, compared to other IMFs. At least the M/Ls must be scaled to a relatively well-defined maximum disk fraction (to better than $\lesssim$ 0.1 dex, or 25%), which carries with it strong implications for scenarios of galaxy formation and evolution.

The above considerations have led to our preferred stellar M/L model: we require that the model reproduces trends in color-based stellar ages and metallicities (Bell & Bower 2000, and §2), properly accounts for the decrease in the color–stellar M/L slope caused by modest bursts of star formation (§4), and has an IMF consistent with maximum disk constraints (this section). These requirements are met by the mass-dependent formation epoch with bursts model, adopting a scaled Salpeter IMF (Fig. 1). We present least-squares fits to the color–stellar M/L trend in Table 1. These fits can be used to estimate a stellar M/L for a spiral galaxy stellar population of a given color, calibrated to maximum disk. If *all* (even very high surface brightness) galaxy disks are sub-maximal, the model fits should be scaled down by an appropriate, constant factor. The fits to our preferred model reproduce the color–M/L trends of the other models with this IMF to better than 0.1 dex (Fig. A10 and Table A3 in Appendix A). These fits are illustrated in panel d of Fig. 1, and in Figs. A9 and A10 by the straight lines. The full models, and fits of stellar M/L against colors not considered in this paper are available from the authors. In particular, fits of the stellar M/L with colors in the Sloan system will become available when the final bandpasses are defined.

6. THE TULLY-FISHER RELATION

TABLE 1
STELLAR M/L AS A FUNCTION OF COLOR FOR THE FORMATION EPOCH MODEL WITH BURSTS, ADOPTING A SCALED SALPETER IMF

Color	a_B	b_B	a_V	b_V	a_R	b_R	a_I	b_I	a_J	b_J	a_H	b_H	a_K	b_K
$B-V$	–0.994	1.804	–0.734	1.404	–0.660	1.222	–0.627	1.075	–0.621	0.794	–0.663	0.704	–0.692	0.652
$B-R$	–1.224	1.251	–0.916	0.976	–0.820	0.851	–0.768	0.748	–0.724	0.552	–0.754	0.489	–0.776	0.452
$V-I$	–1.919	2.214	–1.476	1.747	–1.314	1.528	–1.204	1.347	–1.040	0.987	–1.030	0.870	–1.027	0.800
$V-J$	–1.903	1.138	–1.477	0.905	–1.319	0.794	–1.209	0.700	–1.029	0.505	–1.014	0.442	–1.005	0.402
$V-H$	–2.181	0.978	–1.700	0.779	–1.515	0.684	–1.383	0.603	–1.151	0.434	–1.120	0.379	–1.100	0.345
$V-K$	–2.156	0.895	–1.683	0.714	–1.501	0.627	–1.370	0.553	–1.139	0.396	–1.108	0.346	–1.087	0.314

Note. — $\log_{10}(\mathrm{M/L}) = a_\lambda + b_\lambda \mathrm{Color}$
Note that the stellar M/L values can be estimated for any combination of the above colors by a simple linear combination of the above fits. Note also that if *all* (even very high surface brightness) disks are sub-maximal the above zero points should be modified by subtracting a constant from the above relations.

Having established that galaxy evolution models make robust predictions of a correlation between optical colors and stellar M/Ls, we will now investigate the implications for the TF relation. The TF relation relates the dynamical mass of a galaxy to its luminosity, thus providing a stringent test of theories of galaxy formation and evolution (e.g. Cole et al. 2000; Navarro & Steinmetz 2000b; van den Bosch 2000). However, its power as a test of theories is limited by its passband dependent slope (this assumes linearity of the TF relation, which seems a reasonable assumption over much of the TF relation, although the TF relation may be nonlinear at low galaxy masses: e.g. Matthews, van Driel & Gallagher 1998; McGaugh et al. 2000). The slope of the TF relation varies from around $L \propto V^3$ in the blue to $L \propto V^4$ in the near-IR. Depending on which passband a theory compares its TF relation to, it is possible to have a favorable comparison with one particular TF relation but provide a poor match to a TF relation at a different wavelength. There are, of course, more complex models which include realistic stellar population prescriptions and may be able to reproduce the TF relations at many wavelengths (e.g. Heavens & Jimenez 1999; Cole et al. 2000); however, it would clearly be useful to be able to compare the models with one, unique, passband-independent TF relation.

In this section, we apply the trends in stellar M/L with spiral galaxy color described in Table 1 to the TF relation data of Verheijen (1997) with a dual aim. Firstly, we wish to test the stellar M/Ls derived in § 3 to check if the stellar masses derived from different passbands give consistent results. Secondly, we wish to find out if there is a single, passband-independent TF relation, and if so, what is its slope (assuming a linear TF relation)? The identification of a single, passband-independent TF relation will allow even simplistic models to compare meaningfully with observations without having to construct a complex and realistic SFH model.

6.1. *The data*

Here, we use the TF data obtained by Verheijen (1997) of the Ursa Major Cluster. The Ursa Major Cluster is a nearby (HST Key Project distance D = 20.7 Mpc; Sakai et al. 2000), poor cluster rich in spiral galaxies. The Verheijen data set is particularly suitable for our purposes because it provides accurate magnitudes in *B, R, I* and K' and has accurate rotation velocities from well-resolved HI aperture synthesis rotation curves. We here consider only the rotation velocity at the flat part of the rotation curve ($v_{\rm flat}$): Verheijen (1997) concludes that use of this rotation velocity minimizes the scatter of the TF relation. Furthermore, the rotation velocity at the flat part of the rotation curve is a 'clean' observational quantity at a reasonably well-defined radial range. The HI linewidth is a much more ill-defined quantity, resulting from the interplay of the rotation curve and global HI distribution (even neglecting the influence of warps, asymmetries, kinematic irregularities, and gaseous velocity dispersion). Thus, while the use of linewidth-based TF relations for distance estimation purposes is perfectly valid, the use of linewidths for constructing the *intrinsic* TF relation as a test of galaxy evolution models is far from ideal. Using $v_{\rm flat}$ is much fairer, and better reflects the true relationship between the rotation velocity of a galaxy and the stellar populations in that galaxy.

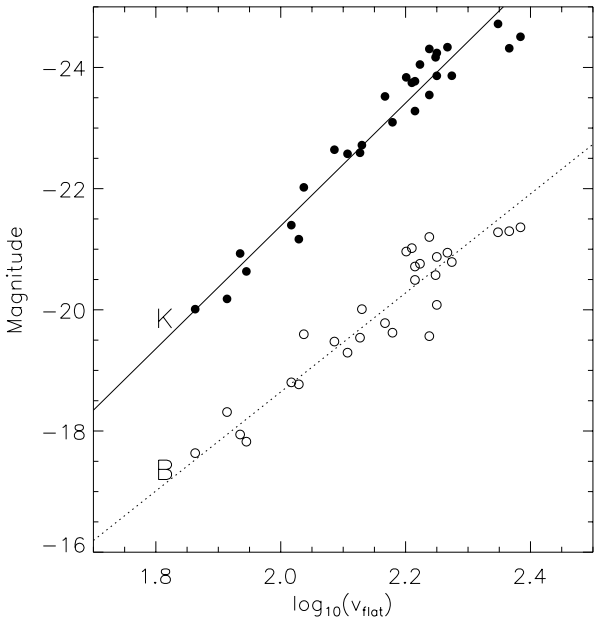

FIG. 7.— The Tully-Fisher relation in *B* and *K* passbands. Solid and open circles denote the data of Verheijen (1997) in *K* and *B* bands respectively, corrected using Tully et al.'s (1998) mass-dependent dust corrections. The lines denote the least squares bisector fits (Isobe et al. 1990) to the mass-dependent dust corrected TF relations.

We correct for foreground galactic extinction assuming a *B* band extinction of 0.08 mag (Schlegel, Finkbeiner & Davis 1998). We further correct for extinction internal to the galaxy following Tully et al. (1998), who determined a galaxy linewidth dependent extinction correction by minimizing scatter around the color–magnitude and TF relation for a sample of 87 galaxies (although the Ursa Major Cluster galaxies form part of the dataset defining the dust correction, meaning that the dust correction we use was partially derived from the TF relation data

we analyze here). According to this recipe, high mass galaxies have a significant extinction correction, whereas low mass galaxies have a negligible extinction correction. We adopt the linewidth-dependent version of this correction. Independent support for a mass-dependent extinction correction comes from de Jong & Lacey (2000), who use a sample of nearly 1000 spiral galaxies to find that high surface brightness (usually luminous) galaxies have optical depths of the order of 1 in their center, but that low surface brightness (usually less luminous) galaxies behave in a nearly transparent manner. For reference, we also tried the mass-independent extinction correction applied by Verheijen (1997) based on the method of Tully & Fouqué (1985).

The TF relations in B and K bands are shown in Fig. 7, as are the best fit least-squares bisectors (see also Table 2). Least squares bisectors (Isobe et al. 1990) are the average of the 'forwards' and 'backwards' fits to the TF relation (which have shallower and steeper slopes than this fit, respectively), and are particularly suitable for probing the intrinsic correlation between two variables. From Table 2 and Fig. 7, it is immediately apparent that the TF relation is shallower in the bluer passbands than in the near-IR, even accounting for magnitude-dependent dust corrections (e.g. Verheijen 1997; Tully et al. 1998). Furthermore, the TF relation constructed using mass-independent dust corrections is shallower than the TF relation constructed using Tully et al.'s (1998) mass-dependent dust corrections: the discrepancy worsens as the passband becomes bluer. The fact that the TF relation steepens at longer wavelengths, even when accounting for mass-dependent dust corrections, is a clear indication that the stellar M/L varies with mass in just the way implied by Fig. 1.

6.2. *The stellar mass TF relation*

To test this possibility in more detail, we adopt the least-squares fit to the variation of stellar M/L with $B-R$ color in B, R, I, and K passbands for the preferred model (formation epoch model with bursts, with a scaled Salpeter IMF). These model relations are used to convert the magnitude-dependent dust-corrected magnitudes into stellar masses, using the dust-corrected $B-R$ color as input. The use of these model relations is suitable: the TF relation from Verheijen (1997) is among the tighest in the literature, implying a minimal contribution from large starbursts. The results are shown in Fig. 8, panel a. Stellar masses derived from B and R passbands are shown as open circles (the masses are identical as the $B-R$ color was used to construct the M/Ls), the I band by crosses, and the K band by filled circles. Least-squares bisector fits of the TF relations are also shown, and given in Table 2.

From panel a of Fig. 8 and Table 2, it is clear that by accounting for the variation in stellar M/L with galaxy color we have demonstrated that there is one passband-independent stellar mass TF relation. The stellar masses determined from $B+R$, I and K band data for the individual galaxies are consistent to within $\sim$ 10% RMS, powerfully demonstrating the utility of this technique and confirming that the trends suggested by our models are indeed consistent with observations. Furthermore, the stellar mass TF relation ($L \propto V^{4.4\pm0.2}$) is steeper than even the K band TF relation ($L \propto V^{4\pm0.2}$). These errors represent only fitting error: errors in IMF and distance scale do not affect the slope of the stellar mass TF relation, and slope errors from adopting fits for different SFH models are ~ 0.2. In addition, the zero point of the stellar mass TF relation is proportional to the distance, as we scale to maximum disk (a $\pm$15% distance uncertainty translates into a ±0.06 dex zero point shift in the stellar mass TF relation).

The scatter in the stellar mass TF relation is somewhat less than 0.5 mag, which is slightly larger than the scatter in the *raw* optical and near-IR TF relations. This is an unavoidable disadvantage of this technique: not only are we making the TF relation steeper (which increases the magnitude scatter if some of the scatter is caused by velocity or distance errors), but we are folding in uncertainties from at least two different passbands' data into the stellar TF relation. However, a slightly enhanced scatter is a relatively modest price to pay: the true strength of this type of analysis is in the recovery of a stellar and/or baryonic mass TF relation which is passband independent.

An interesting test is to consider the effects of the dust correction on the recovered stellar mass TF relation. For example, even assuming that Tully et al.'s (1998) dust correction is appropriate statistically, the dust correction is unlikely to be accurate on a case-by-case basis. Thus it is important to test the effects of choosing a different attenuation for the galaxy. We do this by repeating the above analysis using the mass-independent dust-corrected TF relation (Verheijen 1997), the results of which are shown in panel b of Fig. 8 and Table 2. Comparing the results in Table 2, we confirm the conclusion drawn about reddening in §4.4: the stellar mass TF estimated using a mass-independent dust prescription is almost exactly the same as the mass-dependent dust case. A modest offset of -0.13 dex is found, which stems from a larger blue optical depth in Tully & Fouqué (1985) compared to Tully et al. (1998): this produces bluer de-reddened $B-R$ colors which lead to an overall offset in stellar mass TF relation without a change in slope. One interesting implication of this finding is that we cannot say how much of the decreasing slope of the TF relation with decreasing wavelength is due to dust and how much is due to stellar M/L differences. We expect the effects to be roughly comparable, as Tully et al.'s (1998) corrections seem, at least in a statistical sense, quite appropriate.

6.3. *The baryonic mass TF relation*

When we account for the HI gas fraction to calculate the total known baryon mass (panel c of Fig. 8), we find $m_{\rm baryon} \propto V^{3.5\pm0.2}$ (using an unweighted least-squares bisector fit). Since the baryonic TF relation is of significant astrophysical importance, it is worth discussing the uncertainties in the slope we determine above. We have used an unweighted least-squares bisector: the slope of forwards and backwards fits are ~ 0.15 shallower and steeper repectively. There is an uncertainty of ±0.2 or so depending on which model is used as the preferred model. Furthermore, we have not accounted for the (fairly unconstrained) molecular hydrogen mass fraction: if molecular hydrogen were included it would probably steepen the baryonic TF relation slightly (Young & Knezek 1989). On the other hand, the absolute normalization of the stellar M/L is maximal, which implies that the slope stated above is as steep as is allowed by maximum disk: for reference, adopting a 63% velocity (40% mass) maximal disk following Bottema (1997) or Courteau & Rix (1999) would make the baryonic TF relation slope shallower by 0.5. Also, we have assumed the HST Key Project distance to the Ursa Major Cluster (Sakai et al. 2000). The stellar masses are proportional to distance because we scale to maximum disk; however, the HI masses are affected by the distance D^2. Sakai et al. (2000) estimate around 10% random

TABLE 2
INTERCEPTS AND SLOPES OF THE TF RELATIONS: $L = L_{100}V^{\alpha}$ AND $M = M_{100}V^{\alpha}$

Luminosities	*B*		*R*		*I*		*K*	
Case	$\log_{10} L_{100}/L_{\odot}$	α	$\log_{10} L_{100}/L_{\odot}$	α	$\log_{10} L_{100}/L_{\odot}$	α	$\log_{10} L_{100}/L_{\odot}$	α
Mass-dep dust	9.65 ± 0.03	3.27 ± 0.17	9.60 ± 0.03	3.54 ± 0.16	9.62 ± 0.03	3.77 ± 0.17	9.89 ± 0.03	4.06 ± 0.20
Mass-indep dust	9.84 ± 0.03	2.76 ± 0.15	9.69 ± 0.03	3.18 ± 0.15	9.68 ± 0.03	3.46 ± 0.17	9.88 ± 0.03	3.98 ± 0.20
Masses	*B*		*R*		*I*		*K*	
Case	$\log_{10} M_{100}/M_{\odot}$	α	$\log_{10} M_{100}/M_{\odot}$	α	$\log_{10} M_{100}/M_{\odot}$	α	$\log_{10} M_{100}/M_{\odot}$	α
Stellar mass (MD)	9.51 ± 0.04	4.34 ± 0.22	9.51 ± 0.04	4.34 ± 0.22	9.49 ± 0.04	4.49 ± 0.23	9.49 ± 0.04	4.51 ± 0.26
Stellar mass (MI)	9.38 ± 0.04	4.33 ± 0.23	9.38 ± 0.04	4.33 ± 0.23	9.35 ± 0.04	4.49 ± 0.24	9.37 ± 0.04	4.62 ± 0.25
Baryonic mass (MD)	9.79 ± 0.04	3.45 ± 0.18	9.79 ± 0.04	3.45 ± 0.18	9.78 ± 0.04	3.55 ± 0.19	9.79 ± 0.04	3.51 ± 0.19

Note. — $L_{100}/L_{\odot}$ and $M_{100}/M_{\odot}$ are luminosities and masses in solar units for a galaxy on the TF relation with a $v_{\rm flat}$ of 100 km s^{-1}. Case (MI) uses Tully & Fouqué (1985) mass-independent dust corrections, and Case (MD) uses Tully et al. (1998) mass-dependent dust corrections. Errors denote the uncertainty in the formal fit to the TF relations.

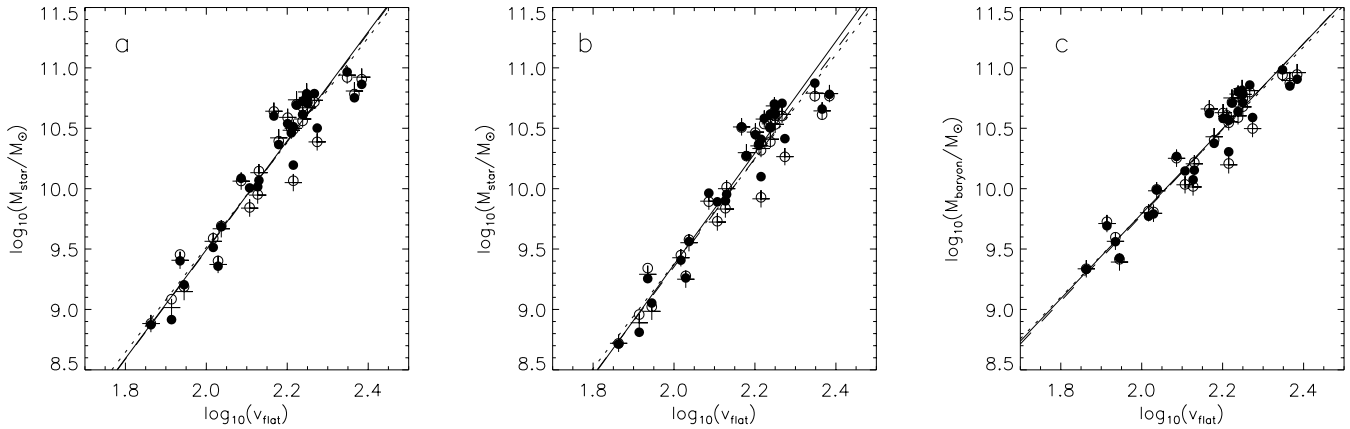

FIG. 8.— TF relations: stellar mass with mass-dependent extinction correction (a), stellar mass with mass-independent extinction correction (b) and baryonic TF relation with mass-dependent extinction correction (c). Masses derived from *B* and *R* data are shown as open circles (the masses are identical as *B*–*R* colors are used to construct the stellar M/Ls), *I* band data by crosses, and *K* band data by solid circles. Least squares bisector fits to each passband's TF relations are presented for the *B* and *R* data (dotted lines), *I* data (dashed lines) and *K* band (solid lines).

and 10% systematic distance uncertainties: the corresponding $\pm$15% total distance error bars lead to slope changes of somewhat less than $\mp$0.1. This suggests that the random and systematic errors for the baryonic TF relation slope should be $\sim$ 0.2 each.

It should be noted that the scatter in the baryonic and stellar mass TF relations can place tight constraints on the allowed variations in IMF at a given rotation velocity. The scatter in the baryonic TF relation is a modest 0.1 dex, and in the stellar mass TF relation, a slightly larger 0.13 dex. Assuming that *all* of the error is due to IMF variations, a FWHM spread of stellar M/Ls of somewhat less than a factor of two is allowed at a given rotation velocity. This is a firm upper limit as we do not account for measurement errors in the luminosity, rotation velocity, the intrinsic depth of the cluster, non-circular potentials (Franx & de Zeeuw 1992), or the intrinsic spread in stellar M/Ls from SFH variations. Taken together with the suggestive tightness of the lower envelope of observational maximum disk stellar M/Ls in Fig. 6 which argues against large IMF variations at a given color, there is little evidence against a universal spiral galaxy IMF.

One interesting comparison that we can perform is with the baryonic TF relation of McGaugh et al. (2000). They use a constant stellar M/L in each passband to construct a baryonic TF relation with a slope which is indistinguishable from 4. They claim that this strongly rules out CDM-like models. We disagree with their result for the slope by around 2σ (even including systematic error): adopting our slope of 3.5 ± 0.2 (random) $\pm$ 0.2 (systematic), the case against the basic relationship $m \propto V_{\rm halo}^3$ predicted by simple CDM models is much weaker (e.g. van den Bosch 2000; Navarro & Steinmetz 2000b).

This disagreement is at first sight somewhat surprising, as accounting for the larger stellar M/Ls and dust extinctions of redder galaxies would steepen the baryonic TF relation, relative to one constructed assuming color-independent stellar M/Ls and dust correction. However, the difference can be traced to a combination of three effects. Firstly, and most importantly, McGaugh et al. (2000) use values of stellar M/L which are around 30–40% larger than ours (at a typical color for a luminous spiral galaxy), and assume a distance 25% shorter than the one we adopt. This accounts for most of the difference in baryonic TF relation slope. Secondly, McGaugh et al. (2000) use linewidths to construct their baryonic TF relation. For a variety of reasons outlined earlier, we chose to use the more physically-motivated rotation velocities at the flat part of the rotation curve: this leads to a shallower TF relation by perhaps as much as 0.2 in terms of the slope (Verheijen 1997, Chapter 5, his Table 7). Finally, we lack galaxies with rotation velocities much lower than 80 km s^{-1}: at present, there is no sample of low mass galaxies with sufficiently accurate rotation velocities and photometry to construct accurate $v_{\rm flat}$ and stellar mass estimates. The inclusion of low mass galaxies may steepen the TF relation, or indicate that

at low masses the TF relation is non-linear (e.g. Matthews, van Driel & Gallagher 1998).

7. CONCLUSIONS

Under the assumption of a universal spiral galaxy IMF, we have used stellar population synthesis models in conjunction with simplified spiral galaxy evolution models to argue that there are substantial variations in stellar M/L in optical and near-IR passbands, and that these M/L variations are strongly correlated with stellar population colors. The variations in stellar M/L also correlate with other galaxy properties (albeit with more scatter) such that, on average, low surface brightness, high gas fraction and low luminosity galaxies have lower stellar M/Ls than high surface brightness, low gas fraction, bright galaxies. The changes in stellar M/Ls over a plausible range of galaxy parameters amount to a factor of about 7 in B, 3 in I, and 2 in K band. In addition, because the central regions of galaxies are often redder than their outer regions, the inner regions of galaxies are likely to have larger stellar M/Ls than the outer regions of galaxies.

This strong correlation between color and stellar M/L is robust to uncertainties in stellar population and galaxy evolution modeling, including the effects of modest bursts of recent star formation. Larger bursts, which are correspondingly more rare and are typically selected against in spiral galaxy studies (as evidenced by the modest scatter in our TF relation), may depress the stellar M/L from our expectations by up to 0.5 dex, at most. In addition, because dust both dims and reddens the light from galaxies, uncertainties in the exact amount of dust do not significantly affect the stellar mass estimate for a given galaxy. The stellar IMF remains the primary uncertainty, implying that these trends are relative in a robust sense, but the absolute normalization is somewhat uncertain.

We analyzed observed K band maximum disk stellar M/Ls from Verheijen (1997) to place the relative stellar M/Ls which we estimate in this paper on the maximum allowed scale. We find that a Salpeter IMF is ruled out by this analysis if the Ursa Major Cluster is placed at the HST Key Project distance of 20.7 Mpc, and that modification of the low-mass end of the IMF is required. We find that the observed maximum disk stellar M/Ls follow the trend suggested by the models, which lends independent support for our models, implies that a fraction of high surface brightness galaxies are reasonably close to maximum disk, and suggests a universal spiral galaxy stellar IMF.

We apply these maximum disk-scaled trends in stellar M/L with galaxy color to investigate the underlying nature of the TF relation. We find that, using mass-dependent dust extinction corrections and the color-dependent stellar M/Ls it is possible to estimate stellar masses from different passbands which are consistent at better than the 10% level. The slope of the stellar mass TF relation of the Ursa Major Cluster sample is 4.4 ± 0.2, using an least-squares bisector fit. Including the contribution from the HI mass, we find that the slope of the baryonic TF relation of the Ursa Major Cluster is 3.5 ± 0.2 (random) $\pm$ 0.2 (systematic), adopting an unweighted bisector fit. The slope will be shallower, if all disks are substantially sub-maximal. This is considerably shallower than the baryonic TF of McGaugh et al. (2000), who advocate $L \propto V^{4\pm0.1}$. We attribute the bulk of the difference to a difference in distance scales and stellar M/L normalization.

We thank Stacy McGaugh for asking us for improved stellar M/L estimates for spiral galaxies, which started us off on this project. We thank all of the stellar population modelers who provided us with their models, and often spent a considerable effort helping us better understand the models. We thank Roelof Bottema, Stephane Courteau, Stacy McGaugh and the anonymous referee for helpful comments. E.F. Bell was supported by NASA grant NAG5-8426 and NSF grant AST-9900789. Support for R.S. de Jong was provided by NASA through Hubble Fellowship grant #HF-01106.01-A from the Space Telescope Science Institute, which is operated by the Association of Universities for Research in Astronomy, Inc., under NASA contract NAS5-26555.

This research has made use of NASA's Astrophysics Data System Abstract Service. This research has made use of the NASA/IPAC Extragalactic Database (NED) which is operated by the Jet Propulsion Laboratory, California Institute of Technology, under contract with the National Aeronautics and Space Administration.

REFERENCES

Bell, E. F., & Bower, R. G. 2000, MNRAS, 319, 235
Bell, E. F., & de Jong, R. S. 2000, MNRAS, 312, 497
Bessel, M. S. 1979, PASP, 91, 589
Bottema, R. 1993, A&A, 275, 16
Bottema, R. 1997, A&A, 328, 517
Bottema, R. 1999, A&A, 348, 77
Brinchmann, J., & Ellis, R. S. 2000, ApJ, 536, 77
Bruzual, A. G., & Charlot, S. 2001, in preparation
Cole, S., Lacey, C. G., Baugh C. M., Frenk, C. S. 2000, MNRAS, in press (astro-ph/0007281)
Courteau, S., & Rix, H.-W. 1999, ApJ, 513, 561
Cox, A. N., Editor, 2000, "Allen's Astrophysical Quantities", 4th Ed. (Springer-Verlag, New York)
de Blok, W. J. G., & McGaugh, S. S. 1998, ApJ, 508, 132
de Jong, R. S. 1996, A&A, 313, 377
de Jong, R. S. & Lacey, C. 2000, ApJ, in press (astro-ph/0008071)
Disney, M. J., Davies, J. I., Phillipps, S. 1989, MNRAS, 239, 939
Fioc, M., & Rocca-Volmerange, B. 2001, in preparation
Franx, M., & de Zeeuw, T. 1992, ApJ, 392, 47
Fukugita, M., Hogan, C. J., Peebles, P. J. E. 1998, ApJ, 503, 518
Heavens, A. F., & Jimenez, R. 1999, MNRAS, 305, 770
Isobe, T., Feigelson, E. D., Akritas, M. G., Babu, G. J. 1990, ApJ, 364, 104
Kennicutt Jr., R. C. 1983, ApJ, 272, 54
Kennicutt Jr., R. C. 1998, ApJ, 498, 181
Kodama, T., & Arimoto, N. 1997, A&A, 320, 41
Kroupa, P., Tout, C. A., Gilmore, G. 1993, MNRAS, 262, 545
Kroupa, P. 2000, MNRAS, in press (astro-ph/0009005)
Larson, R. B. 1999, in Star Formation 1999, ed. T. Nakamoto (Nobeyama Radio Observatory), 336
Liu, M. C., Charlot, S., Graham, J. R. 2000, ApJ, in press (astro-ph/0004367)
Matthews, L. W., van Driel, W., Gallagher, J. S. III 1998, AJ, 116, 2196
McGaugh, S. S., Schombert, J. M., Bothun, G. D., de Blok, W. J. G. 2000, ApJ, 533, 99
Milgrom, M., & Braun, E. 1988, ApJ, 334, 130
Moore, B., Governato, F., Quinn, T., Stadel, J., Lake, G. 1998, ApJ, 499, L5
Navarro, J. F., & Steinmetz, M. 2000a, ApJ, 528, 607
Navarro, J. F., & Steinmetz, M. 2000b, ApJ, 538, 477
Pagel, B. E. J. 1998, "Nucleosynthesis and Chemical Evolution of Galaxies" (Cambridge University Press, Cambridge)
Parodi, B. R., Saha, A., Sandage, A., Tammann, G. A. 2000, ApJ, 540, 634
Portinari, L., & Chiosi, C. 1999, A&A, 350, 827
Prantzos, N., & Boissier, S. 2000, MNRAS, 313, 338
Ratnam, C., & Salucci, P. 2000, preprint (astro-ph/0008121)
Rocha-Pinto, H. J., Scalo, J., Maciel, W. J., Flynn, C. 2000, A&A, 358, 869
Sakai, S., et al. 2000, ApJ, 529, 698
Salasnich, B., Girardi, L., Weiss, A., & Chiosi, C. 2000, A&A, 361, 1023
Salpeter, E. E. 1955, ApJ, 121, 61
Scalo, J. M. 1986, Fundam. Cosmic Phys., 11, 1
Schlegel, D. J., Finkbeiner, D. P., Davis, M. 1998 ApJ, 500, 525
Schmidt, M. 1959 ApJ, 129, 243
Schulz, J., Fritze-von Alvensleben, U., Fricke, K. J. 2001, in preparation
Somerville, R. S., & Primack, J. R. 1999, MNRAS, 310, 1087
Swaters, R. A. 1999, PhD thesis, University of Groningen
Swaters, R. A., Madore, B. F., Trewhella, M. 2000, ApJ, 531, L107
Thuan, T. X., Izotov, Y. I., Foltz, C. B. 1999, ApJ, 525, 105
Tinsley, B. M. 1980, Fundamentals of Cosmic Physics, 5, 287
Tully, R. B., & Fisher, J. R. 1977, A&A, 54, 661

Tully, R. B., & Fouqué, P. 1985, ApJS, 58, 67
Tully, R. B., Pierce, M. J., Huang, J.-S., Saunders, W., Verheijen, M. A. W., Witchalls, P. L. 1998, AJ, 115, 2264
Tully, R. B., & Pierce, M. J. 2000, ApJ, 533, 744
van Albada, T. S., Bachall, J. N., Begeman, K., Sancisi, R. 1985, ApJ, 295, 305
van Albada, T. S., & Sancisi, R. 1986, Phil. Trans. R. Soc. Lond. A, 320, 447
van den Bosch, F. C. 2000, ApJ, 530, 177
van den Bosch, F. C., Robertson, B. E., Dalcanton, J. J., de Blok, W. J. G. 2000, AJ, 119, 1579
Verheijen, M. A. W. 1997, PhD thesis, Univ. of Groningen
Weiner, B. J., Williams, T. B., van Gorkom, J. H., Selwood, J. A. 2000, ApJ, in press (astro-ph/0008204)
Witt, A. N., Thronson Jr., H. A., & Capuano Jr., J. M. 1992, ApJ, 393, 611
Worthey, G. 1994, ApJS, 95, 107
Young, J. S., & Knezek, P. M. 1989, ApJ, 347, 55L

APPENDIX

MODEL TABLES

In this appendix we present plots of the stellar M/Ls of the preferred model (the mass-dependent formation epoch model with bursts, with a scaled Salpeter IMF) against six colors (Fig. A9) and plots of the stellar M/L against $B-R$ color for six different models (Fig. A10). We also present least-squares fits to the variation of stellar M/L of a variety of different galaxy evolution and SPS models with a wide range of colors (Tables A3 and A4 respectively). Further discussion of these tables and figures are presented in the text.

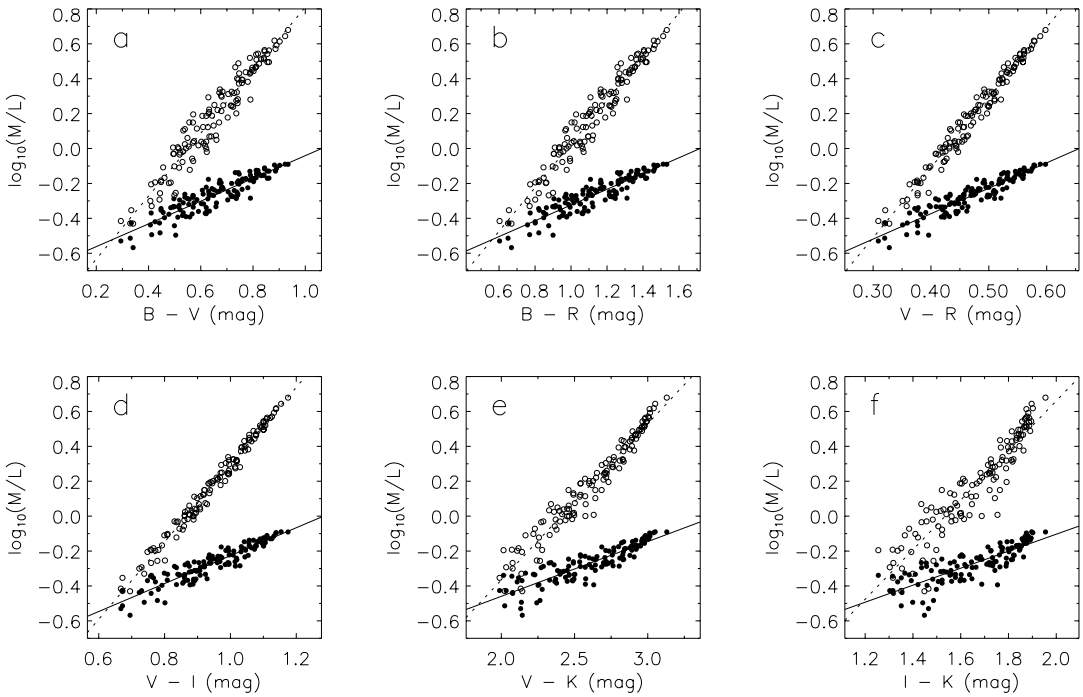

FIG. A9.— Trends in stellar M/L for the formation epoch model with bursts in K (filled circles) and B band (open circles) with $B-V$ (a), $B-R$ (b), $V-R$ (c), $V-I$ (d), $V-K$ (e), and $I-K$ (f) color. We also show the least-squares fit to the variations of stellar M/L with color for the B (dotted line) and K band stellar M/L (solid line).

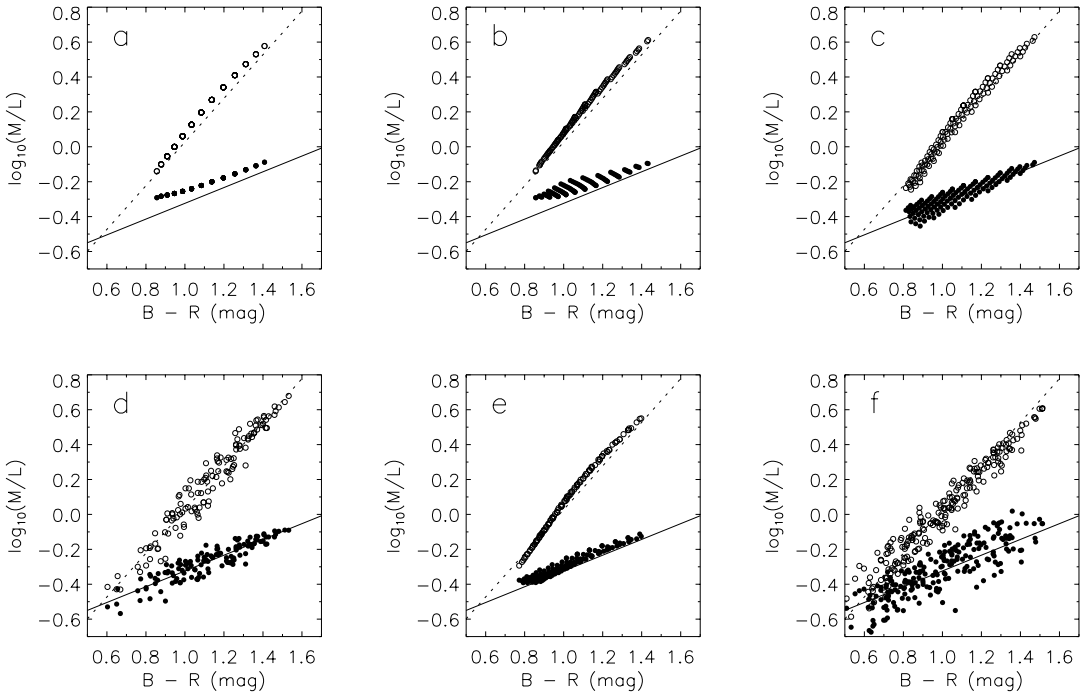

FIG. A10.— Trends in stellar M/L with $B-R$ color for six different galaxy evolution models in K (filled circles) and B band (open circles) for the closed box model (a), outflow model (b), mass-dependent formation epoch model (c), mass-dependent formation epoch model with bursts (d), infall model (e), and Cole et al. (2000) heirarchical model (f). We also show the least-squares fit to the variations of stellar M/L with $B-R$ color of the mass-dependent formation epoch with bursts model for the B (dotted line) and K band (solid line). The Cole et al. (2000) model adopts a Kennicutt (1983) IMF and a 38% brown dwarf fraction, which results in a similar zero point to the scaled-down Salpeter IMF we adopt.

TABLE A3

STELLAR M/L AS A FUNCTION OF COLOR FOR THE SCALED SALPETER IMF

Model	a_B	b_B	a_V	b_V	a_R	b_R	a_I	b_I	a_J	b_J	a_H	b_H	a_K	b_K
						$B-V$								
Closed box	–1.019	1.937	–0.759	1.537	–0.681	1.346	–0.631	1.170	–0.540	0.767	–0.553	0.632	–0.554	0.540
Infall	–1.113	2.065	–0.853	1.665	–0.772	1.468	–0.723	1.290	–0.658	0.907	–0.679	0.777	–0.692	0.699
Outflow	–1.026	1.954	–0.766	1.554	–0.685	1.357	–0.634	1.179	–0.527	0.741	–0.536	0.600	–0.534	0.500
Dynamical time	–0.990	1.883	–0.730	1.483	–0.650	1.289	–0.601	1.114	–0.514	0.704	–0.528	0.569	–0.531	0.476
Formation epoch	–1.110	2.018	–0.850	1.618	–0.770	1.425	–0.724	1.257	–0.659	0.878	–0.683	0.757	–0.694	0.676
Form. epoch: bursts	–0.994	1.804	–0.734	1.404	–0.660	1.222	–0.627	1.075	–0.621	0.794	–0.663	0.704	–0.692	0.652
Cole et al. (2000)	–0.888	1.758	–0.628	1.358	–0.565	1.132	–0.525	0.981	–0.550	0.801	–0.618	0.718	–0.654	0.696
						$B-R$								
Closed box	–1.236	1.312	–0.932	1.042	–0.832	0.912	–0.762	0.793	–0.626	0.519	–0.623	0.427	–0.613	0.364
Infall	–1.334	1.386	–1.032	1.119	–0.930	0.986	–0.861	0.867	–0.754	0.608	–0.760	0.520	–0.764	0.467
Outflow	–1.236	1.313	–0.933	1.045	–0.832	0.913	–0.761	0.793	–0.604	0.496	–0.598	0.400	–0.583	0.332
Dynamical time	–1.195	1.270	–0.892	1.001	–0.791	0.870	–0.723	0.752	–0.590	0.474	–0.589	0.382	–0.581	0.319
Formation epoch	–1.333	1.365	–1.030	1.095	–0.929	0.965	–0.865	0.851	–0.757	0.594	–0.767	0.512	–0.769	0.457
Form. epoch: bursts	–1.224	1.251	–0.916	0.976	–0.820	0.851	–0.768	0.748	–0.724	0.552	–0.754	0.489	–0.776	0.452
Cole et al. (2000)	–1.121	1.130	–0.811	0.875	–0.717	0.730	–0.657	0.633	–0.657	0.516	–0.713	0.461	–0.746	0.447
						$V-I$								
Closed box	–1.771	2.104	–1.359	1.674	–1.207	1.466	–1.087	1.274	–0.835	0.830	–0.791	0.679	–0.755	0.578
Infall	–1.882	2.191	–1.478	1.772	–1.323	1.563	–1.206	1.372	–0.988	0.954	–0.955	0.810	–0.935	0.723
Outflow	–1.743	2.072	–1.341	1.653	–1.188	1.445	–1.069	1.253	–0.786	0.772	–0.737	0.615	–0.692	0.503
Dynamical time	–1.714	2.035	–1.304	1.607	–1.150	1.398	–1.032	1.207	–0.781	0.757	–0.739	0.606	–0.703	0.503
Formation epoch	–1.931	2.234	–1.513	1.797	–1.356	1.584	–1.241	1.397	–1.017	0.972	–0.989	0.835	–0.965	0.744
Form. epoch: bursts	–1.919	2.214	–1.476	1.747	–1.314	1.528	–1.204	1.347	–1.040	0.987	–1.030	0.870	–1.027	0.800
Cole et al. (2000)	–1.674	1.865	–1.249	1.456	–1.088	1.220	–0.977	1.056	–0.901	0.843	–0.924	0.745	–0.943	0.714
						$V-J$								
Closed box	–1.574	0.993	–1.204	0.791	–1.071	0.693	–0.969	0.602	–0.756	0.391	–0.725	0.319	–0.698	0.271
Infall	–1.740	1.054	–1.365	0.854	–1.224	0.753	–1.117	0.660	–0.917	0.454	–0.889	0.382	–0.872	0.338
Outflow	–1.453	0.920	–1.113	0.735	–0.989	0.643	–0.895	0.557	–0.665	0.335	–0.633	0.263	–0.599	0.211
Dynamical time	–1.524	0.952	–1.156	0.753	–1.022	0.655	–0.921	0.566	–0.708	0.353	–0.679	0.281	–0.651	0.232
Formation epoch	–1.780	1.072	–1.392	0.863	–1.250	0.761	–1.146	0.670	–0.944	0.463	–0.923	0.396	–0.903	0.350
Form. epoch: bursts	–1.903	1.138	–1.477	0.905	–1.319	0.794	–1.209	0.700	–1.029	0.505	–1.014	0.442	–1.005	0.402
Cole et al. (2000)	–1.854	1.141	–1.397	0.896	–1.215	0.752	–1.080	0.647	–0.949	0.496	–0.948	0.427	–0.953	0.402
						$V-H$								
Closed box	–1.782	0.840	–1.371	0.669	–1.217	0.586	–1.096	0.509	–0.838	0.330	–0.791	0.269	–0.753	0.228
Infall	–1.962	0.889	–1.546	0.721	–1.384	0.636	–1.257	0.557	–1.011	0.382	–0.966	0.321	–0.939	0.284
Outflow	–1.641	0.776	–1.264	0.621	–1.121	0.543	–1.009	0.470	–0.731	0.282	–0.684	0.221	–0.639	0.176
Dynamical time	–1.725	0.805	–1.317	0.638	–1.161	0.555	–1.042	0.479	–0.783	0.298	–0.737	0.238	–0.699	0.196
Formation epoch	–2.027	0.916	–1.592	0.737	–1.425	0.650	–1.300	0.572	–1.050	0.395	–1.012	0.337	–0.981	0.298
Form. epoch: bursts	–2.181	0.978	–1.700	0.779	–1.515	0.684	–1.383	0.603	–1.151	0.434	–1.120	0.379	–1.100	0.345
Cole et al. (2000)	–2.142	0.961	–1.627	0.756	–1.410	0.635	–1.246	0.546	–1.070	0.415	–1.047	0.356	–1.043	0.333
						$V-K$								
Closed box	–1.738	0.761	–1.336	0.607	–1.187	0.531	–1.069	0.462	–0.820	0.299	–0.776	0.244	–0.740	0.207
Infall	–1.931	0.811	–1.522	0.658	–1.363	0.580	–1.238	0.508	–0.996	0.348	–0.953	0.292	–0.926	0.258
Outflow	–1.583	0.696	–1.218	0.557	–1.081	0.487	–0.974	0.421	–0.708	0.252	–0.664	0.197	–0.622	0.157
Dynamical time	–1.682	0.728	–1.283	0.577	–1.132	0.502	–1.016	0.433	–0.766	0.270	–0.723	0.215	–0.687	0.177
Formation epoch	–1.990	0.832	–1.562	0.670	–1.399	0.590	–1.277	0.520	–1.032	0.358	–0.996	0.305	–0.966	0.270
Form. epoch: bursts	–2.156	0.895	–1.683	0.714	–1.501	0.627	–1.370	0.553	–1.139	0.396	–1.108	0.346	–1.087	0.314
Cole et al. (2000)	–2.125	0.891	–1.615	0.701	–1.400	0.590	–1.235	0.506	–1.051	0.380	–1.026	0.324	–1.019	0.301

$\log_{10}(\mathrm{M/L}) = a_\lambda + b_\lambda \mathrm{Color}$

The Cole et al. (2000) model adopts a Kennicutt (1983) IMF and a 38% brown dwarf fraction, which results in a similar zero point to the scaled-down Salpeter IMF we adopt. Note that the stellar M/L values can be estimated for any combination of the above colors by a simple linear combination of the above fits.

TABLE A4

STELLAR M/L AS A FUNCTION OF COLOR FOR DIFFERENT SPS MODELS

Model	a_B	b_B	a_V	b_V	a_R	b_R	a_I	b_I	a_J	b_J	a_H	b_H	a_K	b_K
			$B-V$			$Z = 0.008$								
Bruzual & Charlot, Salpeter IMF	–0.63	1.54	–0.37	1.14	–0.30	0.97	–0.27	0.83	–0.33	0.68	–0.39	0.62	–0.43	0.60
Bruzual & Charlot, Scaled Salpeter IMF	–0.78	1.54	–0.52	1.14	–0.46	0.97	–0.43	0.83	–0.48	0.68	–0.54	0.62	–0.59	0.60
Bruzual & Charlot, Modified Salpeter IMF	–0.91	1.53	–0.65	1.13	–0.58	0.97	–0.56	0.84	–0.61	0.68	–0.67	0.61	–0.71	0.60
Bruzual & Charlot 96, Scalo IMF	–0.85	1.48	–0.59	1.08	–0.52	0.91	–0.49	0.79	–0.56	0.64	–0.63	0.57	–0.65	0.56
Kodama & Arimoto, Salpeter IMF	–0.56	1.46	–0.30	1.06	–0.24	0.91	–0.22	0.76	–0.26	0.61	–0.36	0.55	–0.38	0.53
Schulz et al., Salpeter IMF	–0.59	1.55	–0.33	1.15	–0.26	0.98	–0.29	0.86	–0.60	0.76	–0.51	0.75	–0.65	0.77
PÉGASE, Salpeter IMF	–0.57	1.51	–0.31	1.11	–0.24	0.95	–0.19	0.76	–0.25	0.65	–0.33	0.60	–0.38	0.59
PÉGASE, $x = -1.85$ IMF	–0.25	1.40	0.01	1.00	0.09	0.82	0.11	0.65	0.05	0.55	–0.03	0.49	–0.07	0.48
PÉGASE, $x = -0.85$ IMF	–0.87	1.75	–0.61	1.35	–0.56	1.20	–0.42	0.90	–0.47	0.79	–0.53	0.70	–0.59	0.71
			$B-V$			$Z = 0.02$								
Bruzual & Charlot, Salpeter IMF	–0.51	1.45	–0.25	1.05	–0.19	0.88	–0.17	0.76	–0.28	0.58	–0.36	0.53	–0.42	0.52
Bruzual & Charlot, Scaled Salpeter IMF	–0.66	1.45	–0.40	1.05	–0.34	0.88	–0.33	0.76	–0.43	0.58	–0.51	0.53	–0.57	0.52
Bruzual & Charlot, Modified Salpeter IMF	–0.79	1.43	–0.53	1.03	–0.47	0.87	–0.46	0.75	–0.55	0.58	–0.63	0.53	–0.69	0.51
Bruzual & Charlot 96, Scalo IMF	–0.74	1.40	–0.48	1.00	–0.42	0.84	–0.40	0.73	–0.49	0.51	–0.58	0.45	–0.61	0.43
Kodama & Arimoto, Salpeter IMF	–0.44	1.40	–0.18	1.00	–0.12	0.84	–0.12	0.70	–0.19	0.53	–0.30	0.48	–0.33	0.45
Schulz et al., Salpeter IMF	–0.49	1.46	–0.23	1.06	–0.16	0.89	–0.20	0.77	–0.59	0.61	–0.48	0.61	–0.64	0.62
PÉGASE, Salpeter IMF	–0.47	1.45	–0.21	1.05	–0.15	0.89	–0.12	0.71	–0.23	0.59	–0.34	0.55	–0.39	0.54
PÉGASE, $x = -1.85$ IMF	–0.15	1.36	0.11	0.96	0.18	0.79	0.19	0.62	0.09	0.49	–0.02	0.44	–0.07	0.44
PÉGASE, $x = -0.85$ IMF	–0.77	1.65	–0.51	1.25	–0.47	1.11	–0.35	0.85	–0.46	0.72	–0.55	0.65	–0.62	0.65
			$B-R$			$Z = 0.008$								
Bruzual & Charlot, Salpeter IMF	–0.84	1.08	–0.52	0.80	–0.43	0.68	–0.39	0.59	–0.42	0.48	–0.47	0.43	–0.51	0.42
Bruzual & Charlot, Scaled Salpeter IMF	–0.99	1.08	–0.68	0.80	–0.59	0.68	–0.54	0.59	–0.57	0.48	–0.63	0.43	–0.67	0.42
Bruzual & Charlot, Modified Salpeter IMF	–1.12	1.08	–0.81	0.80	–0.72	0.68	–0.68	0.59	–0.70	0.48	–0.75	0.44	–0.80	0.42
Bruzual & Charlot 96, Scalo IMF	–1.05	1.04	–0.74	0.76	–0.65	0.64	–0.60	0.56	–0.64	0.45	–0.70	0.40	–0.73	0.39
Kodama & Arimoto, Salpeter IMF	–0.77	1.05	–0.45	0.76	–0.36	0.65	–0.33	0.55	–0.35	0.44	–0.44	0.40	–0.45	0.38
Schulz et al., Salpeter IMF	–0.79	1.08	–0.48	0.80	–0.39	0.68	–0.40	0.60	–0.70	0.53	–0.61	0.52	–0.75	0.54
PÉGASE, Salpeter IMF	–0.78	1.08	–0.47	0.79	–0.38	0.68	–0.30	0.54	–0.35	0.46	–0.42	0.42	–0.47	0.42
PÉGASE, $x = -1.85$ IMF	–0.42	0.97	–0.11	0.70	–0.02	0.57	0.02	0.46	–0.02	0.38	–0.09	0.34	–0.13	0.33
PÉGASE, $x = -0.85$ IMF	–1.18	1.29	–0.85	0.99	–0.77	0.89	–0.58	0.66	–0.61	0.58	–0.65	0.52	–0.72	0.52
			$B-R$			$Z = 0.02$								
Bruzual & Charlot, Salpeter IMF	–0.73	1.03	–0.41	0.74	–0.32	0.63	–0.29	0.54	–0.36	0.41	–0.44	0.38	–0.49	0.37
Bruzual & Charlot, Scaled Salpeter IMF	–0.88	1.03	–0.56	0.74	–0.48	0.63	–0.44	0.54	–0.52	0.41	–0.59	0.38	–0.65	0.37
Bruzual & Charlot, Modified Salpeter IMF	–1.01	1.02	–0.69	0.74	–0.60	0.62	–0.57	0.54	–0.64	0.41	–0.71	0.38	–0.77	0.37
Bruzual & Charlot 96, Scalo IMF	–0.95	1.00	–0.63	0.71	–0.54	0.60	–0.50	0.52	–0.56	0.37	–0.65	0.32	–0.67	0.31
Kodama & Arimoto, Salpeter IMF	–0.65	1.00	–0.33	0.72	–0.25	0.60	–0.22	0.50	–0.27	0.38	–0.38	0.35	–0.40	0.32
Schulz et al., Salpeter IMF	–0.69	1.02	–0.38	0.74	–0.29	0.62	–0.31	0.54	–0.67	0.43	–0.57	0.43	–0.73	0.44
PÉGASE, Salpeter IMF	–0.70	1.04	–0.38	0.75	–0.29	0.64	–0.23	0.51	–0.32	0.43	–0.42	0.39	–0.48	0.39
PÉGASE, $x = -1.85$ IMF	–0.33	0.95	–0.02	0.67	0.07	0.55	0.10	0.44	0.02	0.34	–0.08	0.31	–0.13	0.31
PÉGASE, $x = -0.85$ IMF	–1.08	1.22	–0.74	0.92	–0.67	0.82	–0.51	0.62	–0.59	0.53	–0.67	0.48	–0.74	0.48
			$V-I$			$Z = 0.008$								
Bruzual & Charlot, Salpeter IMF	–1.53	2.01	–1.04	1.49	–0.87	1.27	–0.77	1.09	–0.73	0.88	–0.75	0.80	–0.78	0.78
Bruzual & Charlot, Scaled Salpeter IMF	–1.69	2.01	–1.19	1.49	–1.03	1.27	–0.92	1.09	–0.88	0.88	–0.91	0.80	–0.94	0.78
Bruzual & Charlot, Modified Salpeter IMF	–1.85	2.07	–1.34	1.53	–1.18	1.31	–1.07	1.13	–1.02	0.92	–1.05	0.83	–1.08	0.81
Bruzual & Charlot 96, Scalo IMF	–1.76	2.10	–1.25	1.53	–1.08	1.29	–0.98	1.13	–0.95	0.91	–0.98	0.81	–1.00	0.79
Kodama & Arimoto, Salpeter IMF	–1.49	1.95	–0.98	1.42	–0.81	1.21	–0.71	1.02	–0.65	0.81	–0.71	0.74	–0.71	0.70
Schulz et al., Salpeter IMF	–1.82	2.15	–1.25	1.60	–1.04	1.36	–0.98	1.20	–1.20	1.05	–1.10	1.03	–1.26	1.07
PÉGASE, Salpeter IMF	–1.25	1.70	–0.81	1.25	–0.67	1.07	–0.54	0.85	–0.55	0.74	–0.60	0.67	–0.65	0.67
PÉGASE, $x = -1.85$ IMF	–0.98	1.62	–0.51	1.16	–0.34	0.96	–0.24	0.76	–0.23	0.63	–0.29	0.57	–0.32	0.56
PÉGASE, $x = -0.85$ IMF	–1.18	1.57	–0.85	1.22	–0.78	1.09	–0.58	0.82	–0.61	0.71	–0.66	0.64	–0.72	0.64
			$V-I$			$Z = 0.02$								
Bruzual & Charlot, Salpeter IMF	–1.50	1.99	–0.97	1.44	–0.80	1.21	–0.70	1.04	–0.68	0.80	–0.72	0.73	–0.77	0.71
Bruzual & Charlot, Scaled Salpeter IMF	–1.65	1.99	–1.12	1.44	–0.95	1.21	–0.85	1.04	–0.83	0.80	–0.88	0.73	–0.93	0.71
Bruzual & Charlot, Modified Salpeter IMF	–1.81	2.04	–1.27	1.47	–1.09	1.24	–0.99	1.07	–0.97	0.83	–1.01	0.75	–1.06	0.73
Bruzual & Charlot 96, Scalo IMF	–1.71	2.06	–1.17	1.47	–1.00	1.24	–0.90	1.07	–0.84	0.75	–0.89	0.67	–0.91	0.63
Kodama & Arimoto, Salpeter IMF	–1.42	1.87	–0.88	1.34	–0.71	1.13	–0.61	0.94	–0.57	0.71	–0.64	0.65	–0.65	0.61
Schulz et al., Salpeter IMF	–1.73	2.02	–1.13	1.47	–0.92	1.23	–0.86	1.07	–1.11	0.84	–1.01	0.85	–1.18	0.86
PÉGASE, Salpeter IMF	–1.25	1.72	–0.78	1.25	–0.63	1.06	–0.50	0.85	–0.55	0.70	–0.63	0.65	–0.68	0.64
PÉGASE, $x = -1.85$ IMF	–0.93	1.61	–0.44	1.14	–0.28	0.93	–0.17	0.74	–0.20	0.58	–0.27	0.53	–0.32	0.52
PÉGASE, $x = -0.85$ IMF	–1.24	1.63	–0.87	1.24	–0.79	1.10	–0.60	0.84	–0.66	0.71	–0.74	0.65	–0.81	0.65

TABLE A4
CONTINUED

Model	a_B	b_B	a_V	b_V	a_R	b_R	a_I	b_I	a_J	b_J	a_H	b_H	a_K	b_K
			$V-J$			$Z = 0.008$								
Bruzual & Charlot, Salpeter IMF	–1.98	1.32	–1.37	0.98	–1.15	0.84	–1.01	0.72	–0.92	0.58	–0.93	0.53	–0.96	0.51
Bruzual & Charlot, Scaled Salpeter IMF	–2.13	1.32	–1.52	0.98	–1.31	0.84	–1.16	0.72	–1.08	0.58	–1.08	0.53	–1.11	0.51
Bruzual & Charlot, Modified Salpeter IMF	–2.28	1.35	–1.66	1.00	–1.45	0.85	–1.31	0.74	–1.22	0.60	–1.22	0.54	–1.25	0.53
Bruzual & Charlot 96, Scalo IMF	–2.24	1.35	–1.60	0.98	–1.38	0.83	–1.24	0.73	–1.15	0.58	–1.16	0.52	–1.18	0.51
Kodama & Arimoto, Salpeter IMF	–1.87	1.29	–1.26	0.94	–1.05	0.80	–0.91	0.67	–0.81	0.54	–0.85	0.49	–0.85	0.46
Schulz et al., Salpeter IMF	–3.40	1.58	–2.42	1.17	–2.04	1.00	–1.86	0.88	–1.97	0.77	–1.86	0.76	–2.05	0.79
PÉGASE, Salpeter IMF	–1.86	1.31	–1.26	0.97	–1.06	0.83	–0.85	0.66	–0.82	0.57	–0.85	0.52	–0.89	0.51
PÉGASE, $x = -1.85$ IMF	–1.52	1.23	–0.89	0.88	–0.66	0.73	–0.49	0.58	–0.45	0.48	–0.48	0.43	–0.51	0.42
PÉGASE, $x = -0.85$ IMF	–1.82	1.24	–1.35	0.96	–1.23	0.86	–0.92	0.65	–0.90	0.56	–0.92	0.51	–0.99	0.51
			$V-J$			$Z = 0.02$								
Bruzual & Charlot, Salpeter IMF	–1.99	1.24	–1.32	0.90	–1.09	0.76	–0.95	0.65	–0.87	0.50	–0.90	0.46	–0.95	0.45
Bruzual & Charlot, Scaled Salpeter IMF	–2.14	1.24	–1.48	0.90	–1.25	0.76	–1.11	0.65	–1.03	0.50	–1.06	0.46	–1.10	0.45
Bruzual & Charlot, Modified Salpeter IMF	–2.29	1.27	–1.62	0.92	–1.39	0.77	–1.25	0.67	–1.17	0.52	–1.19	0.47	–1.23	0.46
Bruzual & Charlot 96, Scalo IMF	–2.04	1.15	–1.41	0.82	–1.20	0.69	–1.08	0.60	–0.97	0.42	–1.00	0.37	–1.01	0.35
Kodama & Arimoto, Salpeter IMF	–1.82	1.20	–1.17	0.86	–0.95	0.72	–0.81	0.60	–0.72	0.46	–0.78	0.41	–0.78	0.39
Schulz et al., Salpeter IMF	–3.11	1.30	–2.13	0.94	–1.76	0.79	–1.59	0.68	–1.68	0.54	–1.59	0.55	–1.76	0.55
PÉGASE, Salpeter IMF	–1.94	1.26	–1.28	0.92	–1.06	0.78	–0.85	0.62	–0.83	0.52	–0.89	0.48	–0.94	0.47
PÉGASE, $x = -1.85$ IMF	–1.52	1.16	–0.86	0.82	–0.62	0.67	–0.44	0.53	–0.41	0.42	–0.46	0.38	–0.51	0.37
PÉGASE, $x = -0.85$ IMF	–1.98	1.23	–1.44	0.94	–1.29	0.83	–0.98	0.64	–0.99	0.54	–1.04	0.49	–1.11	0.49
			$V-H$			$Z = 0.008$								
Bruzual & Charlot, Salpeter IMF	–2.39	1.17	–1.67	0.87	–1.42	0.74	–1.23	0.64	–1.10	0.51	–1.09	0.47	–1.12	0.45
Bruzual & Charlot, Scaled Salpeter IMF	–2.54	1.17	–1.83	0.87	–1.57	0.74	–1.39	0.64	–1.26	0.51	–1.25	0.47	–1.27	0.45
Bruzual & Charlot, Modified Salpeter IMF	–2.68	1.18	–1.96	0.88	–1.70	0.75	–1.53	0.65	–1.39	0.52	–1.38	0.48	–1.40	0.46
Bruzual & Charlot 96, Scalo IMF	–2.64	1.16	–1.90	0.85	–1.63	0.72	–1.46	0.63	–1.33	0.50	–1.32	0.45	–1.33	0.44
Kodama & Arimoto, Salpeter IMF	–2.38	1.14	–1.63	0.83	–1.36	0.71	–1.17	0.60	–1.02	0.48	–1.05	0.43	–1.03	0.41
Schulz et al., Salpeter IMF	–3.48	1.53	–2.48	1.13	–2.08	0.96	–1.90	0.85	–2.01	0.75	–1.90	0.73	–2.08	0.76
PÉGASE, Salpeter IMF	–2.34	1.17	–1.61	0.86	–1.36	0.74	–1.09	0.59	–1.02	0.51	–1.03	0.46	–1.08	0.46
PÉGASE, $x = -1.85$ IMF	–1.96	1.10	–1.21	0.79	–0.93	0.65	–0.70	0.52	–0.62	0.43	–0.63	0.39	–0.66	0.38
PÉGASE, $x = -0.85$ IMF	–2.23	1.08	–1.67	0.84	–1.51	0.75	–1.13	0.57	–1.09	0.49	–1.09	0.44	–1.15	0.45
			$V-H$			$Z = 0.02$								
Bruzual & Charlot, Salpeter IMF	–2.44	1.12	–1.65	0.81	–1.37	0.69	–1.19	0.59	–1.06	0.45	–1.07	0.41	–1.11	0.40
Bruzual & Charlot, scaled Salpeter IMF	–2.59	1.12	–1.80	0.81	–1.53	0.69	–1.34	0.59	–1.21	0.45	–1.22	0.41	–1.26	0.40
Bruzual & Charlot, Modified Salpeter IMF	–2.73	1.14	–1.93	0.82	–1.66	0.69	–1.48	0.60	–1.35	0.46	–1.35	0.42	–1.39	0.41
Bruzual & Charlot 96, Scalo IMF	–2.48	1.03	–1.73	0.73	–1.47	0.62	–1.30	0.54	–1.12	0.38	–1.15	0.33	–1.15	0.32
Kodama & Arimoto, Salpeter IMF	–2.34	1.08	–1.54	0.77	–1.26	0.65	–1.07	0.54	–0.92	0.41	–0.96	0.37	–0.95	0.35
Schulz et al., Salpeter IMF	–3.22	1.31	–2.21	0.95	–1.83	0.80	–1.65	0.69	–1.73	0.55	–1.63	0.55	–1.81	0.56
PÉGASE, Salpeter IMF	–2.48	1.14	–1.67	0.83	–1.40	0.71	–1.11	0.56	–1.06	0.47	–1.09	0.43	–1.14	0.43
PÉGASE, $x = -1.85$ IMF	–2.02	1.06	–1.21	0.75	–0.91	0.61	–0.67	0.48	–0.59	0.38	–0.63	0.35	–0.67	0.34
PÉGASE, $x = -0.85$ IMF	–2.47	1.10	–1.82	0.84	–1.63	0.74	–1.24	0.57	–1.21	0.48	–1.24	0.44	–1.31	0.44
			$V-K$			$Z = 0.008$								
Bruzual & Charlot, Salpeter IMF	–2.50	1.13	–1.75	0.84	–1.48	0.71	–1.29	0.61	–1.15	0.50	–1.14	0.45	–1.16	0.44
Bruzual & Charlot, Scaled Salpeter IMF	–2.65	1.13	–1.91	0.84	–1.64	0.71	–1.45	0.61	–1.30	0.50	–1.29	0.45	–1.31	0.44
Bruzual & Charlot, Modified Salpeter IMF	–2.79	1.14	–2.04	0.85	–1.77	0.72	–1.59	0.62	–1.44	0.51	–1.42	0.46	–1.45	0.45
Bruzual & Charlot 96, Scalo IMF	–2.72	1.14	–1.95	0.83	–1.68	0.70	–1.50	0.61	–1.36	0.49	–1.35	0.44	–1.36	0.43
Kodama & Arimoto, Salpeter IMF	–2.38	1.09	–1.63	0.79	–1.36	0.67	–1.17	0.57	–1.02	0.45	–1.05	0.41	–1.03	0.39
Schulz et al., Salpeter IMF	–4.31	1.63	–3.09	1.21	–2.61	1.03	–2.36	0.91	–2.42	0.80	–2.30	0.79	–2.50	0.81
PÉGASE, Salpeter IMF	–2.51	1.16	–1.74	0.85	–1.47	0.73	–1.17	0.58	–1.10	0.50	–1.10	0.46	–1.15	0.45
PÉGASE, $x = -1.85$ IMF	–2.09	1.08	–1.30	0.77	–1.00	0.64	–0.76	0.50	–0.67	0.42	–0.68	0.38	–0.71	0.37
PÉGASE, $x = -0.85$ IMF	–2.45	1.10	–1.84	0.85	–1.66	0.76	–1.25	0.57	–1.19	0.50	–1.18	0.45	–1.25	0.45
			$V-K$			$Z = 0.02$								
Bruzual & Charlot, Salpeter IMF	–2.59	1.09	–1.76	0.79	–1.46	0.67	–1.27	0.57	–1.12	0.44	–1.12	0.40	–1.16	0.39
Bruzual & Charlot, Scaled Salpeter IMF	–2.74	1.09	–1.91	0.79	–1.62	0.67	–1.42	0.57	–1.27	0.44	–1.28	0.40	–1.32	0.39
Bruzual & Charlot, Modified Salpeter IMF	–2.88	1.10	–2.04	0.80	–1.75	0.67	–1.56	0.58	–1.41	0.45	–1.41	0.41	–1.45	0.40
Bruzual & Charlot 96, Scalo IMF	–2.53	0.98	–1.76	0.70	–1.49	0.59	–1.33	0.51	–1.14	0.36	–1.16	0.32	–1.16	0.30
Kodama & Arimoto, Salpeter IMF	–2.35	1.02	–1.55	0.73	–1.27	0.62	–1.08	0.51	–0.92	0.39	–0.97	0.35	–0.96	0.33
Schulz et al., Salpeter IMF	–3.87	1.34	–2.68	0.97	–2.23	0.81	–1.99	0.71	–2.00	0.56	–1.91	0.56	–2.09	0.57
PÉGASE, Salpeter IMF	–2.67	1.13	–1.81	0.82	–1.51	0.70	–1.21	0.56	–1.13	0.46	–1.17	0.43	–1.22	0.42
PÉGASE, $x = -1.85$ IMF	–2.17	1.04	–1.31	0.73	–0.99	0.60	–0.73	0.48	–0.64	0.38	–0.68	0.34	–0.72	0.33
PÉGASE, $x = -0.85$ IMF	–2.71	1.10	–1.99	0.84	–1.78	0.75	–1.36	0.57	–1.31	0.48	–1.33	0.44	–1.40	0.44

$\log_{10}(\mathrm{M/L}) = a_\lambda + b_\lambda \mathrm{Color}$

Note that the stellar M/L values can be estimated for any combination of the above colors by a simple linear combination of the above fits.